Ancient TL

LDAC: An Excel-based program for luminescence equivalent dose and burial age calculations

Peng Liang[1,2,3*] and Steven L. Forman[2]

[1] Department of Geography, School of Earth Sciences, Zhejiang University, Hangzhou 310027, China
[2] Geoluminescence Dating Research Lab., Department of Geosciences, Baylor University, Waco, TX 76798, USA
[3] Institute of Geology and Geophysics, Chinese Academy of Sciences, Beijing 100029, China

*Corresponding Author: LiangPeng@mail.iggcas.ac.cn or LiangPeng2012@live.cn

Received: August 14, 2019; in final form: January 14, 2020

Abstract

In the past 20 years optically stimulated luminescence (OSL) dating has advanced as a well-established geochronometer for dating Quaternary sediments. Currently, there are powerful calculation platforms for specific calculations, such as the R package 'Luminescence' and the web-based dose rate calculator DRAC. However, the community lacks a self-contained computational synthesis that can process equivalent dose and dose-rate calculations to avoid unnecessary data exchange among multiple-platforms that may inadvertently propagate errors. Thus, we have developed a unified calculation program that maintains, archives and synthesizes basic OSL data, applies appropriate statistical models, and dose rate parameters in an updatable platform, to render statistically significant OSL ages. In this paper, the Luminescence Dose and Age Calculator (LDAC) written in Microsoft Visual Basic for Application is presented that can compute final equivalent dose values, the environmental dose rate, and render a final burial OSL age. LDAC incorporates statistical parameters, visual presentations of the equivalent dose distribution, applies well-developed statistical age models, and uses up-to-date dose rate parameters into a computational system using fifteen linked functional routines. Most notably, a Markov chain Monte Carlo slice sampling method was employed to estimate the parameters of the minimum and maximum age models. Also, the statistical basis for error propagation of dose rate and final age was improved. The program is designed to be user-friendly with operations and data entry conveniently executed through a graphical user interface. The operations and calculations are presented with transparency and flexibility, allowing for modification of given values, constants, and algorithms. This computational platform is easily loaded on to a PC and can be used in a Windows environment equipped with Microsoft Excel 2010 or later. The latest version of LDAC can be downloaded along with a user manual at https://github.com/Peng-Liang/LDAC.

Keywords: OSL dating; equivalent dose; statistical age models; dose rate; LDAC; Microsoft VBA

1. Introduction

An accurate and precise chronology for sedimentary processes and the enclosure of associated fossils or artifacts is a cornerstone of the geosciences. Optically Stimulated Luminescence (OSL) dating since 1985 has evolved significantly as an accurate dating technique, providing improved chronologic control for the past 200 ka (Huntley et al., 1985; Wintle, 2008; Wintle & Adamiec, 2017). This geochronometer, based on the principles of radiation dosimetry, measures the burial time since mineral grains, such as quartz and K-feldspar, were last exposed to sunlight (Aitken 1998, p. 6–36; Murray & Wintle 2000; Murray & Wintle 2003; Wintle & Murray 2006; Preusser et al. 2009). An important value in OSL dating is the equivalent dose (D_e), which is the estimate of the ionizing radiation dose received during the burial

period (in Grays; Gy) after solar resetting (Aitken 1998, p. 6–36). An OSL age is calculated by division of the D_e by the estimated dose rate (D_r), which is an evaluation of the exposure rate to ionizing radiation (mGy/yr) from the surrounding sediments and cosmic/galactic sources (Aitken 1998, p. 6–11). OSL dating has advanced significantly in the past thirty years with the advent of single aliquot and grain regeneration (SAR) methods (e.g., Wintle & Murray 2006; Wintle & Adamiec 2017). This geochronometer is most robust when dating sediments that have been well and uniformly solar reset, such as mineral grains from aeolian and littoral environments (e.g., Lang et al. 2003; Forman et al. 2014; Yang et al. 2015; Yang et al. 2019; Lancaster et al. 2016; Tamura et al. 2019). The D_e distribution for well solar reset grains often shows a unimodal distribution, with a low overdispersion value (<0.20) (Forman et al., 2014). However, the D_e can vary substantially for separate aliquots or grains from fluvial and lacustrine environments, reflecting partial solar resetting or incorporation of older grains, mostly exposed in turbid water environments (e.g., Aitken 1998, p. 143–175; Arnold et al. 2007; Cunningham & Wallinga 2012; Hesse et al. 2018). Thus, the D_e distribution of variably solar reset grains often exhibits a multi-modal distribution with a high overdispersion (>0.30). Commonly, the youngest D_e population for grains is the closest to the actual age for partially solar-reset sediments (e.g., Cunningham & Wallinga 2012; Hesse et al. 2018).

Fortunately, there are several statistical models such as the central, minimum, maximum, and finite mixture age models that have been developed to deconvolute D_e populations that reflect the time since sediment deposition and shielding from further sunlight exposure (Galbraith & Green, 1990; Galbraith et al., 1999; Galbraith & Roberts, 2012). In turn, the environmental D_r is a required assessment for dating, which is defined by ten separate variables reflecting complex, ionizing-radiation conditions during the burial period (Aitken 1998, p. 37–57; Durcan et al. 2015). Thus, there is a need for a calculation platform that synthesizes D_e data, incorporates appropriate statistical models, and D_r parameters in a self-consistent manner, which can be easily updated with future refinements in constants, statistical analyses, and data visualization. Several well-appointed calculation programs have been developed for specific D_e and D_r computations that serve the luminescence dating community well (e.g., Grün 2009; Kreutzer et al. 2012; Peng et al. 2013; Durcan et al. 2015; Burow et al. 2016). For example, a highly flexible **R** script-based computational package, `'Luminescence'` (Kreutzer et al., 2012, 2018), was designed to further analyze the luminescence data from SAR measurements. This package was integrated into the latest version of the Analyst luminescence software (v4.57), which supports modeling functions and graphing routines (Duller, 2018). However, the **R**`'Luminescence'` package lacks a visual interface with user interactions through the **R** programming environment. As a partial remedy for this platform a graphical user interface (GUI) does exist through `''RLumShiny''` (Burow et al., 2016), but the graphic-presentation functionality is limited. Desktop- or web-based programs, such as the AGE (Grün, 2009) and DRAC (Durcan et al., 2015), have been developed to address the challenges of dose rate calculations. Nevertheless, one must exchange data among multiple programs to obtain the final age, which increases the risk of involuntary errors and inconsistent error analyses. To our knowledge, the luminescence dating community lacks an integrated and interfaced calculation platform to determine OSL ages such as software Calib (Stuiver et al., 2019) or OxCal (Ramsey, 1995, 2017) for radiocarbon dating, ISOPLOT (Ludwig, 1988) or IsoplotR (Vermeesch, 2018) for U-Pb dating, and CRONUS (Balco et al., 2008) or iceTEA (Jones et al., 2019) for cosmogenic nuclide dating.

We present an integrated OSL age calculation program with a well-defined statistical foundation, based on the Microsoft Visual Basic for Application (VBA), referred to as 'Luminescence Dose and Age Calculator (LDAC)', to fulfill a computational need for OSL geochronology. The program is a user-friendly OSL-age-computational system based on previously presented statistical analyses, mathematical relations and other formulations (Galbraith, 1988, 1990, 2003; Bailey & Arnold, 2006; Arnold et al., 2009; Grün, 2009; Duller, 2007, 2015; Durcan et al., 2015). The Microsoft Excel platform was chosen to provide the broadest access and accountability for code, constants, and calculations, though certain Monte Carlo based calculations have lag times of ~ 1 minute. LDAC offers a computational platform to determine OSL age estimates with metrics to assess the statistical robustness of equivalent dose data (Bailey & Arnold, 2006; Arnold & Roberts, 2009), the applicability of statistical age models (Galbraith & Roberts, 2012) and with up-to-date dose rate parameters (Adamiec & Aitken, 1998; Guérin et al., 2011; Liritzis et al., 2013; Durcan et al., 2015). Included in this platform are revised computational pathways for determining overdispersion values on small D_e populations (Galbraith & Roberts, 2012), a new slice sampling method to deconvolute subpopulations using the minimum and maximum models (Neal, 2003), and Monte Carlo based-calculations for the final OSL age estimate. This program can be easily updated to improve dose rate determinations, OSL age calculations, enhanced visualizations, and as a platform to encourage inter-laboratory OSL age comparisons. The current version (LDAC v1.0) of this computational scheme with the code is open access to the community at `https://github.com/Peng-Liang/LDAC`, where a video highlights the capabilities of this computation package. We welcome use by the community and comments to improve this nascent computational platform.

2. Architecture of LDAC

LDAC is an Excel VBA-based package to facilitate the assemblage of luminescence age information and associated calculations. This software is applicable for individual equivalent dose measurements using the SAR protocol (e.g., Wintle & Murray 2006). This computational system has two major components for D_e and D_r calculation (Fig. 1),

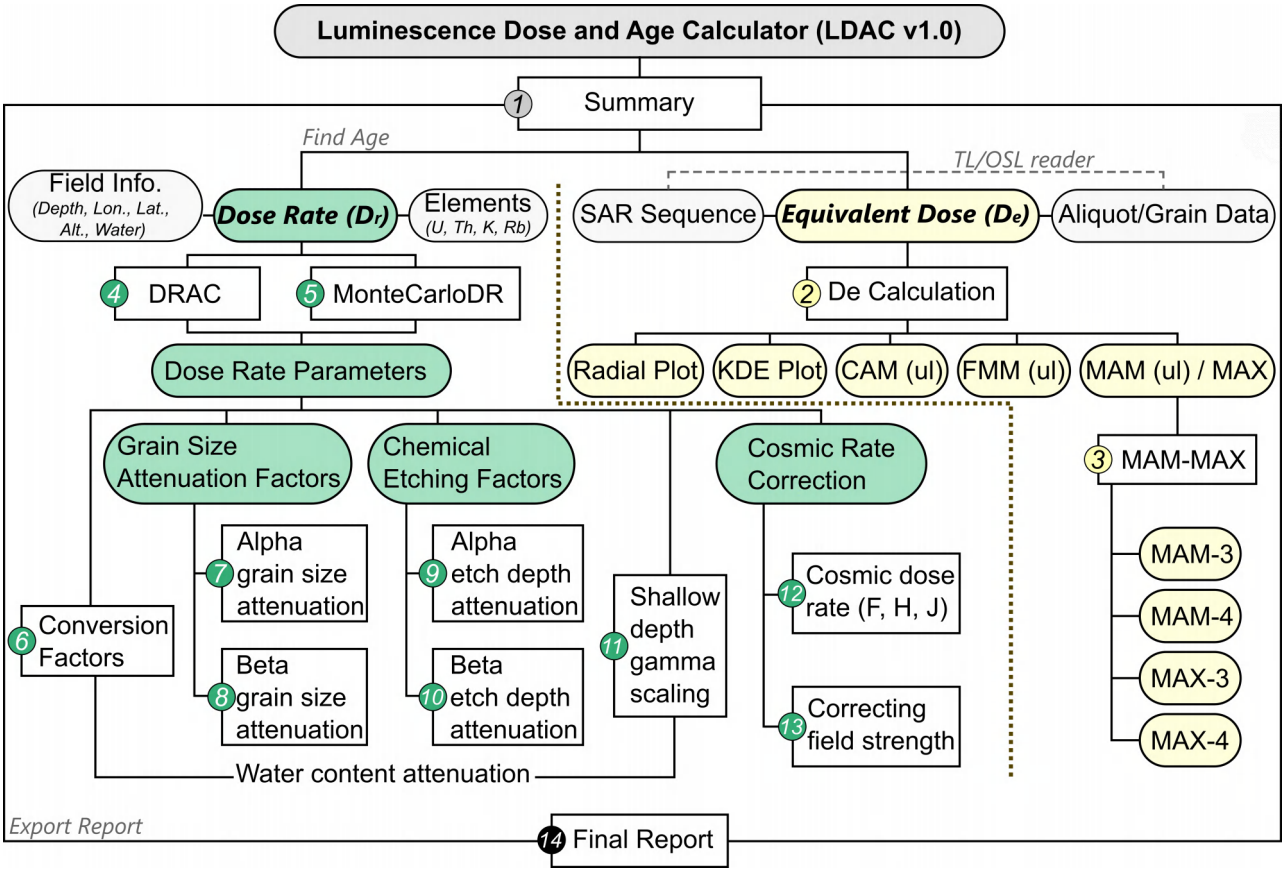

Figure 1. Computational pathways for the Luminescence Dose and Age Calculator (LDAC). The rectangular boxes marked with numbers represent worksheets in LDAC, while the oval frames represent attribute information. The software has two components which are the dose rate calculation system (green) and equivalent dose calculation system (yellow).

based on the following simplified luminescence age equation (Aitken 1998, p. 6–11):

$$Age(yr) = \frac{D_e\,(\mathrm{Gy})}{D_r\left(\frac{\mathrm{Gy}}{\mathrm{yr}}\right)}, \qquad (1)$$

where the D_e is the burial dose accumulated in grains; the D_r is the dose rate that comes from exposure to ionizing radiation from α, β and γ particles in the grain, surrounding sediments, and from cosmic rays (Aitken 1998, p. 37–49). This suite of computations is based on fourteen-linked calculation routines for applying statistical models to determine D_e values and render a corresponding luminescence age (Fig. 1).

The first step to use this computational package is the entry of individual grain or aliquot D_e data, elemental, environmental and contextual information to calculate sample $D_r$which is organized in the "Summary" worksheet (Fig. 1; Supplement A). Subsequent calculations of a final D_e, D_r and an OSL age are presented in succeeding workspaces with these calculations based on data entry on to the "Summary" page (Fig. 1; Supplement A). This "Summary" page allows users to input pertinent information for a sample, such as lab number, field number, sediment type, sample locality and analyst. In turn, there is computation space for D_r information, such as the U, Th, K or K_2O, Rb, water content (mass of water/mass of dry sediment), organic content, grain size, geographical coordinates, elevation, depth, overburden density and a sub-routine to calculate a cosmic dose contribution. Lastly, there are data entry spaces for parameters about the laboratory protocols, including preheat, cut heat, and annealing temperatures, test dose, and irradiation dose cycles (Fig. 1; Supplement A), which are used for keeping a record.

The "Summary" page also has flexible space for the entry of first tier of luminescence data directly imported from the 'Analyst' platform (Duller, 2007, 2018). This data includes calculated individual D_e values for each aliquot or grain (for up to 5000 D_e values) and related parameters such as recycling ratio, percent recuperation (Murray & Wintle, 2000; Wintle & Murray, 2006) with associated errors. Other pertinent diagnostic metrics such as the fast ratio (Durcan & Duller, 2011) and the infrared depletion ratio (Duller, 2003) can also be input. Individual D_e values for single aliquots or grains that fail to meet the data quality assessment metrics (cf. Murray & Wintle 2000; Duller 2003; Durcan & Duller 2011) are marked in a reddish-pink with a toggle choice ('Reject') and are removed from subsequent calculations but stored as part of total aliquots. Designating the 'Transfer'

button transmits the accepted D_e values with standard errors for aliquots/grains into the "De Calculation" page to visualize the D_e data and apply statistical age models.

The "De Calculation" page includes statistical parameters, graphical presentation (see section 3), and parametric statistical models (see section 4) such as common, central, minimum, maximum, and finite mixture age models (Galbraith & Green 1990; Galbraith et al. 1999; Galbraith & Roberts 2012; Fig. 1). Normal and log-normal distributions can be applied to all age models, except the maximum age models, which were only designed for log-transformed data (Olley et al., 2006; Galbraith & Roberts, 2012). LDAC offers two flexible approaches to estimate the uncertainty of overdispersion for the central age model. The first and default option utilizes the formula provided by Galbraith et al. (1999), but this equation is often inappropriate for smaller sample sizes (e.g., <30 aliquots) (Galbraith & Roberts, 2012). An alternative calculation is applied by computing the 95% compatibility interval (CI) of the profile log-likelihood function (Galbraith & Roberts, 2012), when the 'Plot-Lik' checkbox is chosen (see section 4.1). Application of minimum or maximum age models are a separate calculation on a succeeding worksheet entitled "MAM-MAX" (Worksheet 3, Fig. 1). Moreover, two types of diagrams, radial plot (Galbraith, 1988) and kernel density estimate plot (Galbraith & Roberts, 2012), can be created in the "De Calculation" page for data visualization (Fig. 2). The appearance of these graphical displays can be adjusted by users with inputs for decimal places, dot size, dot and curve color, below the plot area in the worksheet "De Calculation", and the dose unit can be chosen either seconds or Grays (worksheet 2 in Fig. 1; Supplement A). Exported figures include sample information such as lab number, the number of aliquots/grains, overdispersion, age model used and final D_e and errors (Fig. 2). Finally, the chosen D_e (tick box) and the designated calculation models will be automatically transferred to the "Summary" page to determine the final OSL age.

Calculation of the cosmic and total environment dose rate, final OSL age, and associated uncertainties (1σ) is actuated by clicking the 'Find Age' button in the "Summary" page (see section 5). The default option for calculating dose rate is modified from the DRAC (v1.2), and the associated uncertainties are propagated in quadrature (Durcan et al., 2015). Propagation of uncertainties through Monte Carlo simulations is also available for the final age calculation in LDAC (see section 5.4). Highlighted dose and age calculation results of the target sample can be compiled as a *.pdf version report via the 'Export Report' button (Fig. 1). This report includes sample identification, dose rate, equivalent dose, sequence information, error analyses, and an associated data-based summary table. Additionally, the relevant graphical presentations will be included in this report if available (worksheet 14 in Fig. 1; Supplement B).

There are additional functionalities in the right-hand corner actuated by the 'Show info', the 'Calibration' and the 'Import' tabs. The 'Show info' allows users to display the underlying basis of the dose-rate calculation and relevant parameters (worksheets 4 to 14, Fig. 1). The 'Calibration' button is used to update the strength of radiation source of the OSL readers in the user's laboratory to compensate for decay changes in source strength. The 'Import' button can transfer data between different versions of LDAC. To familiarize the user with this platform, an example data set is provided after clicking the 'Load Example' button on the "Summary" page.

3. Statistical parameters and graphical presentation of observed D_e values

3.1. Statistical parameters

Statistical parameters may be useful to characterize the D_e distributions for a sample based De values from individual aliquots or grains and may assist in deciphering the depositional environment (Bailey & Arnold, 2006; Arnold & Roberts, 2009). LDAC provides two widely used descriptive statistical parameters, including weighted skewness (Bailey & Arnold, 2006; Arnold & Roberts, 2009) and the chi-square (χ^2) homogeneity test (Galbraith, 2003; Galbraith & Roberts, 2012), to score the original observed data distribution and help to decide which age model is statistically appropriate.

The weighted skewness (c) is calculated as (Bailey & Arnold, 2006):

$$c = \sum_{i=1}^{n} \left\{ w_{\mathrm{ci}} \left(\frac{d_i - \delta}{S_{D_e}} \right)^3 \right\} \frac{1}{\sum_{i=1}^{n} w_{\mathrm{ci}}} \qquad (2)$$

where $w_{\mathrm{ci}} = \left| \frac{1}{\sigma_i / d_i} \right|$, d_i and σ_i are the observed D_e and corresponding standard error for an aliquot or a grain i, respectively; n and s_{D_e} are the total number and standard deviation of all valid observed D_e values. The δ here is the weighted mean of observed D_e values (Arnold & Roberts, 2009) or the central dose value obtained from 'un-logged' central age model (see section 4.1). Note that Eq. 2 is only suitable for original numeric values. When log-transformation is used in data analyses (tick 'Log-Normal'), the following equation is applied (Arnold & Roberts, 2009):

$$c = \sum_{i=1}^{n} \left\{ w_{\mathrm{ci}} \left(\frac{ln(d_i) - \delta}{S_{\ln \mathrm{De}}} \right)^3 \right\} \frac{1}{\sum_{i=1}^{n} w_{\mathrm{ci}}} \qquad (3)$$

where $s_{\ln \mathrm{De}}$ is the standard deviation of the natural logarithm D_e values, δ is the central value obtained from the usual (log-transformed) common or central age model (see section 4.1).

LDAC employs the standard error of skewness σ_c, an approach proposed by Bailey & Arnold (2006), to test the relative statistical significance of the skewness scores calculated by Eq. 2 or Eq. 3. The σ_c is approximated as (Tabachnick & Fidell, 1996):

$$\sigma_c = \sqrt{6/n}. \qquad (4)$$

The modeling investigations of single grains D_e indicate that $\pm\, 2\sigma_c$ can be regarded as the limits for statistically significance of the weighted skewness c (Bailey & Arnold, 2006).

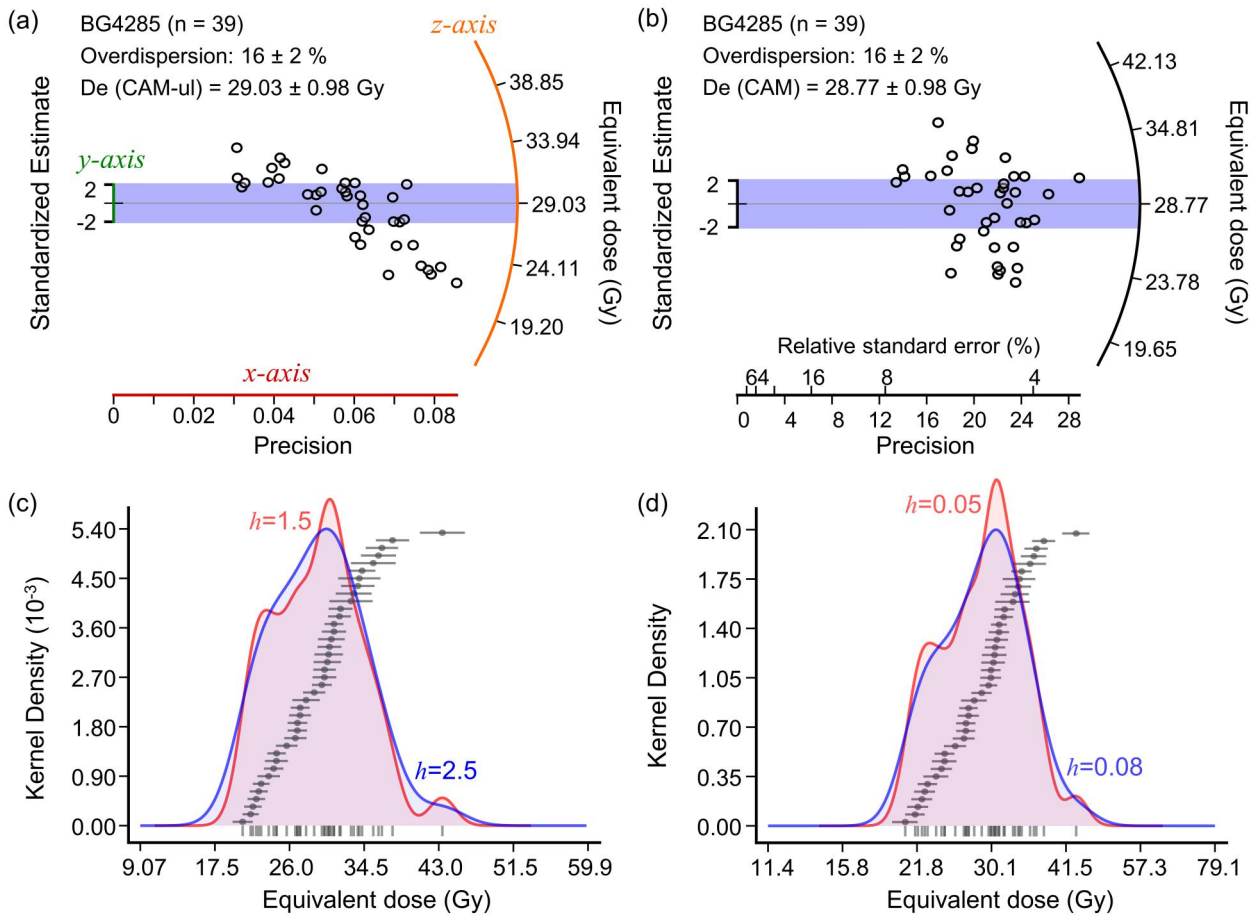

Figure 2. Example figures on "De Calculation" worksheet of radial plots (a, b) and graphs of kernel density estimate (KDE) (c, d) for sample BG4285. Figures (a) and (c) show BG4285 data with normal scale and figures (b) and (d) display the same data with log-transformed scale. The orange and blue colors in (c) and (d) mark the KDE curve with different bandwidth "*h*", revealing potentially different equivalent dose peaks. The grey dots and bars show the empirical cumulative distribution for equivalent dose values and ± 1 standard error.

However, a critical c value of $\pm 1\sigma_c$ is a more meaningful indicator of statistical significance for multi-grain data because of the 'averaging out' effects (Arnold et al., 2007; Arnold & Roberts, 2009). Although LDAC uses $\pm 1\sigma_c$ as a critical skewness value to categorize D_e or log D_e distributions as 'positive' ($c > \sigma_c$), 'negative' ($c < -\sigma_c$) or 'not significant' ($-\sigma_c \leq c \leq \sigma_c$), the original c and σ_c values are also provided in the "De Calculation" page (Supplement A).

LDAC utilizes the 'p-value' of the χ^2 distribution to provide a visual assessment of homogeneity of independent D_e estimates (Galbraith, 2003). This homogeneity test supposes that there are n independent observed values $d_i \pm \sigma_i$, and each d_i is drawn from a normal distribution $N(\mu_i,\ \sigma_i)$. The null hypothesis is that all individual values of μ_i are equal to an unknown common value μ. In this case, the maximum likelihood estimates of $\widehat{\mu}$ under the null hypothesis is:

$$\widehat{\mu} = \frac{\sum_{i=1}^{n} w_i d_i}{\sum_{i=1}^{n} w_i}, \tag{5}$$

where $w_i = \frac{1}{\sigma_i^2}$, and the homogeneity test statistic (G) is defined by:

$$G = \sum_{i=1}^{n} w_i (d_i - \widehat{\mu})^2. \tag{6}$$

Then, a p-value, the probability that a random value drawn from a χ^2 distribution with $n-1$ degrees of freedom is $>G$ (Galbraith, 2003; Galbraith & Roberts, 2012), is calculated according to the G statistic and the degrees of freedom. The smaller the p-value for any given number of observed values, the stronger the evidence to reject the null hypothesis (Galbraith & Roberts, 2012). However, if the p-value is greater than the conventional critical value 0.05 (a small G statistic), then there is insufficient evidence for overdispersion, rather than no overdispersion between observed values (Galbraith, 2003; Galbraith & Roberts, 2012). This homogeneity test can also be applied to evaluate the agreement of paired-age or -dose estimates (Galbraith & Roberts, 2012).

3.2. Graphical presentation

Objective statistical analyses and visual assessments for D_e distributions are critical to evaluate the most appropriate

age model (Galbraith, 1988, 2005, 2010). A useful statistical representation of D_e values is with a radial plot, that displays D_e values against precision (Galbraith, 1988, 2005) and is used widely by the trapped-charge dating community (e.g., Bøtter-Jensen et al. 2003, p. 296–310; Arnold & Roberts 2009; Galbraith & Roberts 2012; Forman 2015; Yang et al. 2015; Guérin et al. 2017). Another useful graphical presentation is the kernel density estimate plot (Sircombe, 2004; Galbraith, 2010; Galbraith & Roberts, 2012; Vermeesch, 2012, 2018; Ramsey, 2017), which is a graphic representation of continuous values that approximates the distribution as a probability density function (Galbraith, 2010).

The radial plot reflects the data distribution, with each value registered independently, where the y-axis is a standardized estimate and the x-axis represents the precision of values (Galbraith, 1988). This plot supposes that there are observed values $d_i \pm \sigma_i$ for aliquot or grain $i = 1, 2, \ldots, n$. The coordinate for each point (x_i, y_i) is calculated by:

$$x_i = \frac{1}{\sigma_i} \text{ and } y_i = \frac{(d_i - d_0)}{\sigma_i}, \tag{7}$$

where d_0 is a convenient reference value (Galbraith & Roberts, 2012). In LDAC, d_0 is the value calculated based on un-logged D_e values by the central age model (CAM-ul) (see section 4.1) and the y scale is truncated at ± 2 standardized estimation (Fig. 2a), which can be used as an aid to evaluate the agreement between any individual value and a reference value (Galbraith & Roberts, 2012). The horizontal line $y = 0$ corresponds to $d_i = d_0$; the ratio y_i/x_i is the slope of the line from the origin point (0, 0) to the target point (x_i, y_i) , which is the difference between an observed value d_i and reference value d_0 (Fig. 2a). The scale of the slope, the z-axis, is displayed as an arc of a circle (Galbraith, 1988, 1990) to yield the radial nature of the plot. When the data is log-transformed, for the observed values d_i with associated standard error σ_i, the Eq (7) is modified to:

$$x_i = \frac{1}{\sigma_i/d_i} \text{ and } y_i = \frac{\ln d_i - \ln d_0}{\sigma_i/d_i}, \tag{8}$$

where d_0 is the value calculated by logarithmic-based central age model (CAM) (see section 4.1). In this case, the precision in x-axis represents the reciprocal of relative standard error and z-axis is in a natural logarithm scale (Fig. 2b).

The kernel density estimate (KDE) for a set of observed values $d_1, d_2, \ldots, d_n$ at x is calculated based on the Gaussian kernel as follows:

$$\text{KDE}(x) = \frac{1}{n}\sum_{i=1}^{n}\left[\frac{1}{h\sqrt{2\pi}}\exp\left(-\frac{1}{2}\left(\frac{x-d_i}{h}\right)^2\right)\right], \tag{9}$$

where h is known as smoothing parameter 'bandwidth' that plays an important role in KDE (Silverman 1998, p. 43–59). As h varies there will be variable resolution of the density curve depicting varying peaks of the data distribution (Silverman 1998, p. 43–59; Galbraith & Roberts 2012; Vermeesch 2012; Fig. 2c, d). The default method for KDE representation is 'adaptive bandwidth' which varies with the density of the data (Botev et al. 2010; Supplement C). This method uses a narrower bandwidth near the dense data distribution and a wider bandwidth near the sparse data distribution (Botev et al., 2010; Vermeesch, 2018). Thus, the resolution of the KDE curve is optimized by the data availability (Vermeesch, 2018). A constant bandwidth for KDE derived from Silverman (1998, p. 45–49) and user-defined values (Supplement C) are also available. Moreover, a probability density function method, where the bandwidth h in Eq. 9 is replaced by the analytical uncertainties σ_i, is provided when the bandwidth method 'PDF plot' is chosen (Supplement C). A continuous KDE curve does not directly reflect the original data distribution, so the individual D_e values with errors are plotted on the KDE graph in rank order as an empirical distribution function (Fig. 2c, d; Galbraith & Roberts 2012). Additionally, the KDE can be calculated with log-transformed data, when d_i in Eq. 9 is altered to $\ln d_i$ (Fig. 2d).

4. Age models for D_e determination

The complexity of depositional processes, environmental microdosimetry, and individual mineral grains response to optical stimulation may result in D_e values measured from separate aliquots or grains exhibiting significant scatter (Jacobs & Roberts, 2007; Arnold & Roberts, 2009; Galbraith & Roberts, 2012; Cunningham & Wallinga, 2012; Guérin et al., 2017). Thus, it is usually inappropriate to analyze such D_e data by assuming a simple Gaussian distribution, by using the weighted average method (Taylor 1997, p. 173–179), known as the common age model (Supplement C; Galbraith 2005, p. 47–50; Galbraith & Roberts 2012). Fortunately, there exists other statistical models that are more appropriate metrics for non-Gaussian data distributions. This section focuses on presenting the logic and mathematical bases for the application of the much used central, minimum and maximum age models to D_e data; the statistical principles of the common and finite mixture age models are discussed in the supplementary information (Supplement C).

4.1. Central age model

The central age model (CAM) is commonly adopted to determine a final D_e value for well solar reset sediments, such as aeolian sand (e.g., Forman et al. 2014; Yang et al. 2015; Hesse et al. 2018; Tamura et al. 2019). The CAM assumes that D_e values are not consistent even if the measurement errors σ_{w_i} are considered, and the natural logarithm of true D_e ($\ln D_e$) values are drawn from a normal distribution with central dose δ and standard deviation σ (Galbraith et al., 1999; Galbraith & Roberts, 2012). The standard deviation σ, also known as overdispersion, denotes an additional dispersion after accounting for within-aliquot/grain measurement errors (Galbraith & Roberts, 2012). The central dose δ and overdispersion σ are estimated with simultaneous evaluation of the following three equations (Galbraith et al., 1999):

$$w_i = \frac{1}{\sigma^2 + {\sigma_{w_i}}^2} \tag{10}$$

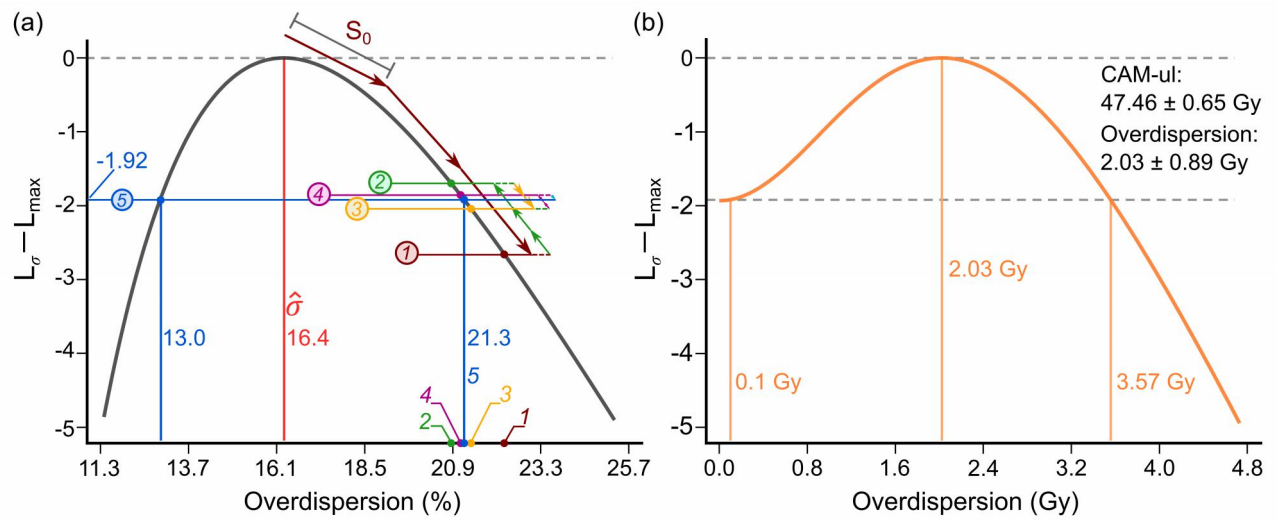

Figure 3. Examples of profile log-likelihood function for the overdispersion in the central age model. (a) Illustration of the algorithm for calculating the standard error of overdispersion based on profile log-likelihood function (BG4285). The limits of 95% comparability interval were calculated by searching the values of σ to fulfill $L_\sigma - L_{\max} = 1.92$ on this profile log-likelihood function. Sequential the calculation entails, first, give an initial step (brown arrow) to cross over the line $L_\sigma - L_{\max} = 1.92$ and find the brown point ①. Then, give a finer step (green arrow) to go back and cross over the line 1.92 again to find the green point ②. Repeat this calculation until a fine limit ⑤, under the tolerance (0.01%), was reached. The calculation of lower limit is same. (b) An example of output shows the profile log-likelihood function for overdispersion parameter σ in the un-logged central age model (CAM-ul); in this case, the overdispersion and associated error are expressed in grays (Gy).

$$\delta = \frac{\sum_{i=1}^{n} w_i d_i}{\sum_{i=1}^{n} w_i} \tag{11}$$

$$\sum_{i=1}^{n} {w_i}^2 (d_i - \delta)^2 = \sum_{i=1}^{n} w_i \tag{12}$$

where d_i and σ_{w_i} are the natural logarithm of observed D_e value and relative standard error for aliquot or grain i, respectively. When overdispersion σ is zero, the CAM is mathematically equivalent to the common age model (Galbraith & Roberts, 2012). These equations are solved by starting with an initial σ = 0.5 (overdispersion is 50%), and calculate w_i for each i based on Eq. 10, and then calculate δ based on Eq. 11; this calculation iterates and updates sequentially with an $\sigma = \sigma(\frac{\sum_{i=1}^{n} {w_i}^2 (d_i-\delta)^2}{\sum_{i=1}^{n} w_i})$. Once the parameters σ and δ satisfy Eq. 12 with $\frac{\sum_{i=1}^{n} {w_i}^2 (d_i-\delta)^2}{\sum_{i=1}^{n} w_i} = 1$ (assuming $w_i \neq 0$), appropriate estimates, $\widehat{\sigma}$ and $\widehat{\delta}$, are derived.

LDAC provides two methods to estimate the standard error of the overdispersion. For large sample populations, the standard error (se) could be approximately (Galbraith et al., 1999):

$$\text{se}\ (\delta) = \sqrt{\frac{1}{\sum_{i=1}^{n} w_i}} \tag{13}$$

$$\text{se}\,(\sigma) = \sqrt{\frac{1}{2\sigma^2 \sum_{i=1}^{n} {w_i}^2}} \tag{14}$$

The above $se(\sigma)$ can be unreliable for smaller sample populations (e.g., < 30) (Galbraith & Roberts, 2012). In this case, an alternative calculation is executed using the 'profile log-likelihood function' to provide an assessment of the standard error of the overdispersion. This method constructs a profile log-likelihood function of L_σ against σ (Galbraith & Roberts, 2012), where

$$L_\sigma = \frac{1}{2} \sum_{i=1}^{n} \left\{ \ln w_i - w_i (d_i - \delta)^2 \right\}. \tag{15}$$

When σ equals the maximum likelihood estimated overdispersion $\widehat{\sigma}$, the L_σ has its maximum value $L_{\max}$ and it decreases as σ departs from $\widehat{\sigma}$. Based on the large-sample maximum likelihood theory and the likelihood-ratio test, approximate boundaries of 95% CI are values of σ for which L_σ is within 1.92 of $L_{\max}$ (Cox 2006, p. 96–106; Galbraith & Roberts 2012). These coarse boundaries are evaluated by searching for threshold values of σ for which $(L_\sigma - L_{\max}) \leq$ -1.92 from $\widehat{\sigma}$ to either direction with an initial step S_0 (e.g., $S_0 = 5\%$ of $\widehat{\sigma}$) in the profile log-likelihood function (Fig. 3a). This calculation is iterated sequentially with 10% of the previous step as a new value (e.g., 10% of S_0) to resolve finer compatibility intervals (Fig. 3a). A symmetric standard error of $\widehat{\sigma}$ is calculated by dividing the length of this 95% CI by 3.92 when the distribution of σ is assumed to be Gaussian (Cox 2006, p. 64–93; Galbraith & Roberts 2012).

A challenge for luminescence dating is that the usual (natural logarithm transformed) CAM may be unsuitable for young sediments (e.g., < 350 a) because of low signal to noise ratio and the preponderance of negative D_e values (Arnold et al., 2009; Galbraith & Roberts, 2012). Consequently, an un-logged central age model (CAM-ul) was de-

signed for samples which contains grains with near-zero or negative D_e values (Arnold et al., 2009). In this case, the d_i is the original D_e values for each aliquot or grain i, and the σ_{w_i} is the absolute rather than relative standard error. The absolute overdispersion and 95% CI is calculated and shown graphically as a profile log-likelihood function (Fig. 3b). If the overdispersion $\widehat{\sigma}$ for CAM-ul equals 0, the estimate δ given by Eq. 11 is mathematically equivalent to 'inverse variance weighted mean' of the observed D_e values (Taylor 1997, p. 173–179; Galbraith & Roberts 2012).

4.2. Minimum age models

4.2.1 Statistical principle of minimum ages models

The minimum age model (MAM) is designed for sediments that contain a mixture of grains with different solar-resetting histories, with inherent varying luminescence emissions (Galbraith et al., 1999; Galbraith & Roberts, 2012). Though mineral grains in a sedimentary unit may have an equivalent burial time, the component grains yield varying equivalent doses, indicating grain populations were not fully solar reset prior to burial (Galbraith et al., 1999; Preusser et al., 2009). These partially bleached sediments are typically characterized by high overdispersion (>0.25) of D_e distributions (Rodnight, 2008; Galbraith & Roberts, 2012). In such cases, the MAM may be most suitable to determine the D_e for the burial period. The MAM assumes that the burial $\ln D_e$ values are drawn from a truncated normal distribution, where γ denotes the lower truncation point and corresponds to the average burial $\ln D_e$ of the well solar-reset grains. The proportion of well-bleached grains is denoted by p; the partially bleached grains have larger doses which are drawn from a truncated normal distribution with parameters μ and σ (Galbraith et al., 1999; Galbraith & Roberts, 2012). Note that if the ln D_e distribution were not truncated, it would have a mean μ and a standard deviation σ as δ and σ for the central age model (Galbraith et al., 1999).

For the MAM, LDAC calculates the probability density function f_i for a ln D_e value d_i based on (Galbraith et al., 1999; Galbraith & Roberts, 2012):

$$s_i{}^2 = \sigma_{w_i}{}^2 + \sigma_b{}^2 \tag{16}$$

$$\mu_* = \frac{\frac{\mu}{\sigma^2} + \frac{d_i}{s_i{}^2}}{\frac{1}{\sigma^2} + \frac{1}{s_i{}^2}} \tag{17}$$

$$\sigma_* = \frac{1}{\sqrt{\frac{1}{\sigma^2} + \frac{1}{s_i{}^2}}} \tag{18}$$

$$f_{1i} = \frac{1}{\sqrt{2\pi s_i{}^2}} \exp\left(-\frac{(d_i-\gamma)^2}{2 s_i{}^2}\right) \tag{19}$$

$$f_{2i} = \frac{1}{\sqrt{2\pi\,(\sigma^2+s_i{}^2)}} \frac{1-\Phi\left(\frac{\gamma-\mu_*}{\sigma_*}\right)}{1-\Phi\left(\frac{\gamma-\mu}{\sigma}\right)} \exp\left(-\frac{(d_i-\mu)^2}{2\,(\sigma^2+s_i{}^2)}\right) \tag{20}$$

$$f_i = p f_{1i} + (1-p) f_{2i} \tag{21}$$

where d_i and σ_{w_i} are the same as the parameters in Eqs. 11 and 12; $\Phi(\bullet)$ is the cumulative distribution function of $N(0,\ 1)$; f_{1i} and f_{2i} are the contribution from the well-bleached component and partially bleached component, respectively. Another important parameter in this age model is σ_b in Eq. 16, which is a likely overdispersion for the expected population of well-bleached grains, such as between-grain variation in a heterogenous dose environment ('hot grains') (Jacobs & Roberts, 2007; Guérin et al., 2015). This σ_b is independent of within-grain or aliquot measurement error and inhomogeneous solar resetting (Galbraith et al., 2005; Cunningham & Wallinga, 2012). An appropriate σ_b is difficult to measure for mixed grain populations with variable D_e but can be assessed from well solar reset mineral grains from the same source (Galbraith & Roberts, 2012). Overestimating or underestimating the σ_b will lead to corresponding older and younger age estimates. In LDAC, we use a default σ_b of 0.11 $\pm$ 0.04 (11 $\pm$ 4%) for multi-grain data consistent with the value recommended by Cunningham & Wallinga (2012). However, it is advised to evaluate σ_b for each sample dated (Galbraith et al., 2005; Cunningham & Wallinga, 2012). Thus, users can input other σ_b values in the "MAM-MAX" worksheet (Supplement A). Hence, the four unknown parameters p, γ, μ and σ in Eqs. 16–21 can be estimated when the log-likelihood L is a maximum, where

$$L(d_i,\ \sigma_{w_i}|p,\ \gamma,\ \mu,\ \sigma) = \sum_{i=1}^{n} \ln f_i. \tag{22}$$

Some data sets with a small number of valid values or less dispersed distributions, may be uncalculatable with the above four-parameters model (MAM-4). Thus, it may be suitable to apply a simpler three parameters model in which $\mu = \gamma$ (MAM-3) (Galbraith et al., 1999). As with the CAM, this natural logarithm-transformed MAM may be unsuitable for sediments that have a D_e <0.50 Gy, with significant zero and negative values which are consistent with zero dose within 2 standard errors (Arnold et al., 2009; Galbraith & Roberts, 2012). In this case, the un-logged minimum age model (MAM-ul) is used, which supposes that the actual D_e instead of $\ln D_e$ values are drawn from a truncated normal distribution, where γ denotes the lower truncation point and corresponds to the average burial D_e of well-bleached grains (Arnold et al., 2009). Thus, the parameters d_i and σ_{w_i} in Eqs. 16–22 are referred to the actual dose and absolute standard error, rather than log-transformed and relative standard error scale. Likewise, the σ_b of MAM-ul in Eq. 16 is the absolute overdispersion (Gy) instead of the relative overdispersion (%) of well-bleached grains.

4.2.2 Markov chain Monte Carlo slice sampling for parameters estimation

There is need for computational tools to estimate the four parameters p, γ, μ and σ for the MAM (Eqs. 16–22). Often these values and associated standard errors are computed numerically through an optimization program such as Fortran program 'minim' (Galbraith et al., 1999) or maximum

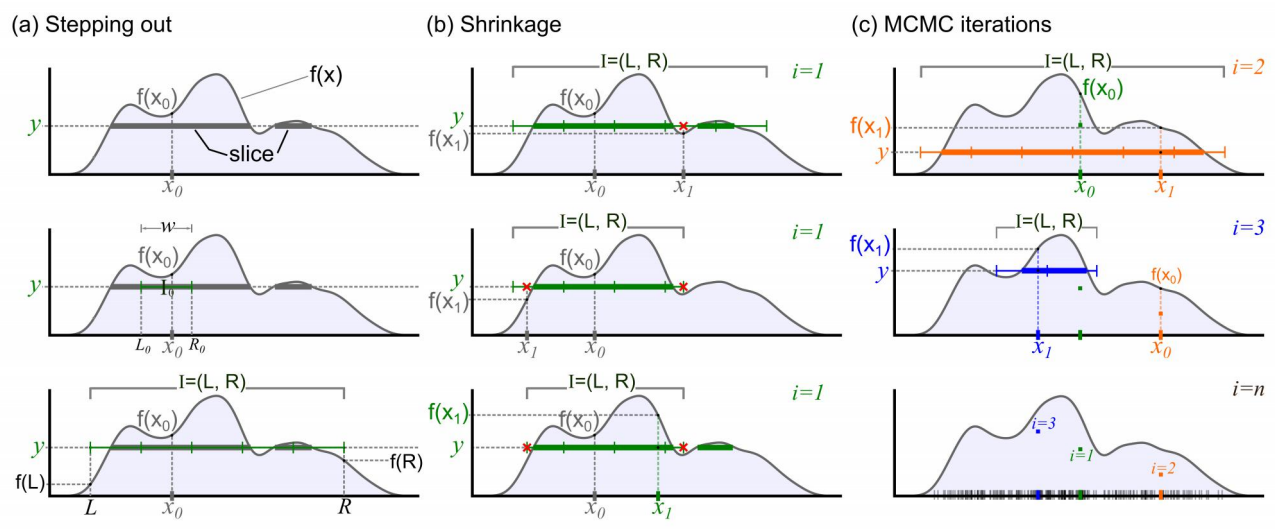

Figure 4. Procedures for estimating the parameters for the minimum age model (Galbraith & Roberts, 2012) using Markov chain Monte Carlo (MCMC) slice sampling method (Neal, 2003). (a) Processes for defining the "slice" (bold line), positioning an initial interval I_0, and expanding the I_0 to $I = (L, R)$ in incremental steps w to include the slices as more as possible. (b) Initiate a calculation at point x_1 uniformly from the interval I until a value is found inside the slice. Values outside the slice (e.g., the red dots "×") are used to shrink the interval. (c) MCMC iterations using the procedures of (a) and (b) to obtain the distribution of f(x).

likelihood estimation package `'bbmle'` in **R** (Bolker & R Development Core Team, 2017). However, these packages are incompatible with an Excel VBA-based computational system. A well-adapted replacement is through 'slice sampling' based on the Markov chain Monte Carlo (MCMC) method (Gilks et al. 1996; Neal 2003; Brooks et al. 2011, p. 215–219; Peng et al. 2013), which was initially used by an **R** package `'numOSL'` to solve the MAM parameters (Peng et al., 2013). The basis of this algorithm is that any unknown distribution can be obtained by sampling uniformly from a region under a probability distribution curve, applying an MCMC algorithm (Neal 2003; Vermeesch 2007; Fig. 4). The procedures of single-variable slice sampling are outlined in Table 1 and shown in Fig. 4 (Neal, 2003).

The advantage of the slice sampling is that it is appropriate for a single-variable distribution (Neal, 2003). This computation is adept at sampling a multivariate distribution such as $L(x)$ in Eq. 21 for $x = (p, \gamma, \mu, \sigma)$, by repeatedly updating each variable in turn (Neal, 2003). This slice sampling method is more efficient through 'stepping out' and 'shrinkage' procedures (Neal, 2003) than the other Markov chain methods such as Gibbs sampling (Gelfand & Smith, 1990) and adaptive-rejection Metropolis sampling methods (Gilks et al., 1995; Vermeesch, 2007). In LDAC, the MCMC slice sampling (Table 1) is used to estimate the maximum likelihood parameters for the MAM, based on Eq. 21 and rotationally update parameters (Table 2).

The fundamental prerequisite for applying the MCMC algorithm to estimate parameters and associated uncertainties for a distribution is that the Markov chain attains convergence states (Gilks et al. 1996; Cowles & Carlin 1996; Neal 2003; Brooks et al. 2011, p. 163–174). Several diagnostic tools can be applied to assess the steps for value convergence (Cowles & Carlin, 1996). In LDAC, trace plot, marginal density, and autocorrelation function (ACF) are employed to evaluate the convergence states of a Markov chain analysis (Fig. 5). A trace plot shows the trajectories at each MCMC iteration and is a straightforward graphic to assess the convergence of a Markov chain (Gilks et al., 1996; Plummer et al., 2006; Philippe et al., 2019). The Markov chain reached a stable state if the trace plot displays a random distribution with a relatively constant mean and variance (Brooks et al. 2011, p. 163–174; Philippe et al. 2019). In LDAC, the default number of iterations is $n = 1800$, which balances the convergence, precision, and efficiency of the MAM calculations. An unsuitable initial value affects the initial behavior of a Markov chain within finite iterations (see Fig. 5). Thus, we use a 'burn-in' strategy (Gilks et al. 1996; Brooks et al. 2011, p. 19–23), which discards the first t iterations of a Markov chain analysis, to reduce the influence of initial values and use exclusively the stationary values for estimation of parameters. Another graphical assessment method is the autocorrelation function, which monitors the correlation between states of the Markov chain (Brooks et al. 2011, p. 163–174). High sampling autocorrelation may result in a biased standard error for Monte Carlo iterations (Gilks et al., 1996). LDAC computations use a conventional 'thinning' method (Gilks et al. 1996; Brooks et al. 2011, p. 163–174), with every kth iteration stored, to reduce autocorrelation between consecutive iterations. The default values for burn-in and thinning in LDAC are 200 and 4, respectively. Consequently, the number of MCMC iterations used for final parameter estimation is $[(n-t)/k]$ (in LDAC, 400). Users can adjust (increase) the default values for Monte Carlo iterations, burn-in inter-

Table 1. The 'stepping out' and 'shrinkage' procedures for Markov chain Monte Carlo (MCMC) slice sampling method for Minimum Age Model calculations.

Step	Calculation	Notes
1	Give an initial value, x_0, and calculate $f(x_0)$;	x_0 and $f(x_0)$ in Fig. 4a
2	Draw an auxiliary value at vertical level, y ,uniformly from $(0,\ f(x_0))$, thereby defining a horizontal 'slice': $S = \{x : y < f(x)\}$;	The bold gray lines in Fig. 4
3	Give a rough estimate, w, for the scale of S (w is estimated prior to slice sampling and keep constant);	Fig. 4
4	Pick randomly an initial interval $I_0 = (L_0,\ R_0)$, which size equals w, containing x_0;	I_0 is the green line in Fig. 4a and the length of $I_0 = w$
5	Expand the initial interval I_0 by 'stepping out' procedure (Neal, 2003) until $f(L)\ \leq y$ and $f(R) \leq y$; we get an interval as $I = (L,\ R)$;	The thin solid green line in Fig. 4a;
6	Draw a new point x_1 uniformly from the interval I using 'shrinkage' method (Neal, 2003). If the $f(x_1) < y$, reject the value, shrink the interval I and repeat the uniform sampling within the new interval again, until $f(x_1) \geq y$.	The rejection points and shrinkage procedures are illustrated in Fig. 4b.
7	Set the new point x_1 as current point x_0 and return to 1.	The MCMC iteration is illustrated in Fig. 4b,c

Table 2. Protocol for applying the single-variable slice sampling method outlined in Table 1 to estimate parameters from a multivariable distribution.

Step	Procedure	Calculation
1	Calculate the lower and upper limits of p, γ, μ, σ;	$p \in [0,\ 1]$; $\gamma \in [\min(d_i),\ max(d_i)]$; $\mu \in [\min(d_i),\ max(d_i)]$; $\sigma \in [0,\ 10]$;
2	Give initial values of p, γ, μ, σ within their range;	$p_0, \gamma_0, \mu_0, \sigma_0$; both default and user-defined values are available;
3	Calculate new points $p_1, \gamma_1, \mu_1, \sigma_1$ using the single-variable slice sampling method and save these values in a matrix $[j,k]$ (j represents the time of iterations; k represents the number of parameters);	$p_1 = \text{slice sampling}\,(L(p_0\|\gamma_0, \mu_0, \sigma_0, d_i, \sigma_{w_i}))$; $\gamma_1 = \text{slice sampling}\,(L(\gamma_0\|p_1, \mu_0, \sigma_0, d_i, \sigma_{w_i}))$; $\mu_1 = \text{slice sampling}\,(L(\mu_0\|p_1, \gamma_1, \sigma_0, d_i, \sigma_{w_i}))$; $\sigma_1 = \text{slice sampling}\,(L(\sigma_0\|p_1, \gamma_1, \mu_1, d_i, \sigma_{w_i}))$;
4	Set $p_1, \gamma_1, \mu_1, \sigma_1$ as new $p_0, \gamma_0, \mu_0, \sigma_0$ and return to 2;	Start Markov chains iteration $j+1$ until hit the limit on iterations.

Note: slice sampling (•) is a single-variable slice sampling calculation function based on Table 1.

actions and thinning to ensure the convergence states are reliably reached. Finally, the central value and 95% CI of the estimated parameters are calculated based on the arithmetic mean, 2.5% and 97.5% quantiles from the stationary MCMC results (Brooks et al. 2011, p. 175–197). The standard errors of parameters are estimated by dividing the length of 95% CI by 3.92 (Cox 2006, p. 64–93; Galbraith & Roberts 2012).

4.2.3 Validation of slice sampling MAM

A simulated data set was fabricated by mixing D_e data of two disparate samples to test the veracity of the slice sampling for resolving the youngest D_e population by the MAM. The first sample is well-bleached quartz grains with an overdispersion of 4 ± 2 % and a D_e (CAM) of 47.7 ± 0.7 Gy (n = 30) (Table 3; Fig. 6a). The second sediment is poorly-bleached and contains three significant D_e components, displaying a high overdispersion (37 ± 3%) with an apparent D_e (CAM) of 158.5 ± 7.1 Gy (n = 70) (Table 3; Fig. 6b). The two simulated sediments have an average relative standard error of 6 ± 1.5% (Fig. 6). The two data sets are combined (n = 100), and the aliquots from each sample are traced by two different colors: red for well solar reset data set and green for the high dispersed data (see Fig. 6c). The overdispersion of this mixed, synthetic sample is 63 ± 5 % and the apparent D_e calculated by CAM is 110.4 ± 7.0 Gy (Fig. 6c).

The slice-sampled MAM approach was tested using the MAM-4 computations in LDAC. A total of 1800 iterations of MCMC slice sampling were implemented. The first 200 iterations of the MCMC were discarded ('burn-in') and ap-

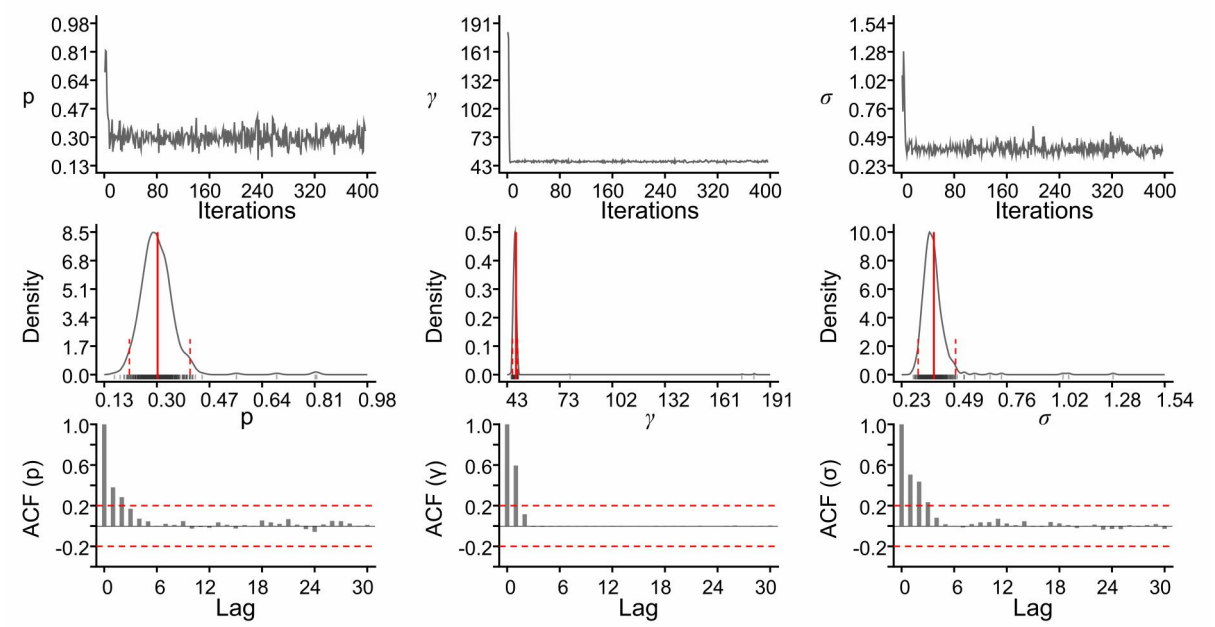

Figure 5. An example of Markov chain Monte Carlo sampling without 'burn-in' and 'thinning' showing graphical diagnostics such as trace plots (upper), marginal densities (middle) and evaluation of autocorrelation (ACF) (lower). There is high autocorrelation until after lag-3 analysis.

plied a data thinning routine of registering every 4th value to avoid autocorrelation. The trace, KDE and autocorrelation plots demonstrate stationarity of the Markov chain analysis (Fig. 7). Finally, 400 iterations (after burn-in and thinning) were used to estimate p, γ, μ and σ and their 95% CI (Table 3; Fig. 7). The default initial values given by MAM-4 in this experiment are $p_0 = 0.5$, $\gamma_0 = 3.93$ (normal scale: 50.91 Gy), $\mu_0 = 4.7$ (normal scale: 109.95 Gy) and $\sigma = 4.87$. The σ_b is 0.0438 $\pm$ 0.0173 which is the overdispersion of the well-bleached component of this synthetic sample (Fig. 6a). The results of this experiment indicate that the slice sampling MAM can reliably separate the lowest synthetic D_e associated with the well solar-reset subpopulation (Table 3).

4.3. Maximum age models

The maximum age model (MAX) was proposed for sediments that are suspected to be disturbed or mixed by processes that lead to partial or full solar resetting of grains post deposition, such as pedogenesis or other biogenic activities (Olley et al., 2006; Galbraith & Roberts, 2012; Ahr et al., 2013). The MAX computation model shares the same assumption and statistical principle with the MAM (section 4.2.1), but the γ is defined as the upper truncation point of the truncated log-normal distribution of true D_e values (Olley et al., 2006; Galbraith & Roberts, 2012). As with the MAM, LDAC provides three and four parameters maximum age models (MAX-3 and MAX-4, respectively) following the method developed by Olley et al. (2006). The same equations and parameters estimation methods as the MAM are used, but the d_i in Eqs. (16-22) is changed to

$$d_i = -\ln \mathrm{De}_i + \ln\left[\mathrm{Max}\left(\mathrm{De}\right)\right], \qquad (23)$$

where De_i is the observed value from single aliquot or grain i, $Max(De)$ is the maximum value of all observed D_es. The purpose of this conversion process is to create a 'mirror image' of the original data distribution (Olley et al., 2006).

Table 3. The results of slice sampling for Minimum Age Model-4 (MAM-4) for the simulated sample.

Parameters	Known values ($\pm$ 1 σ)	MAM-4 estimates (LDAC)	
		Asymmetric CI (95%)	Standard error ($\pm$ 1 σ)
p	0.30	$0.300^{+0.10}_{-0.08}$	0.300 $\pm$ 0.045
γ	47.66 $\pm$ 0.65 Gy	$47.59^{+1.46}_{-1.30}$ Gy	47.59 $\pm$ 0.71 Gy
μ	158.49 $\pm$ 7.10 Gy	$157.17^{+14.08}_{-16.37}$ Gy	157.17 $\pm$ 7.77 Gy
σ	0.37 $\pm$ 0.03	$0.386^{+0.07}_{-0.06}$	0.386 $\pm$ 0.033

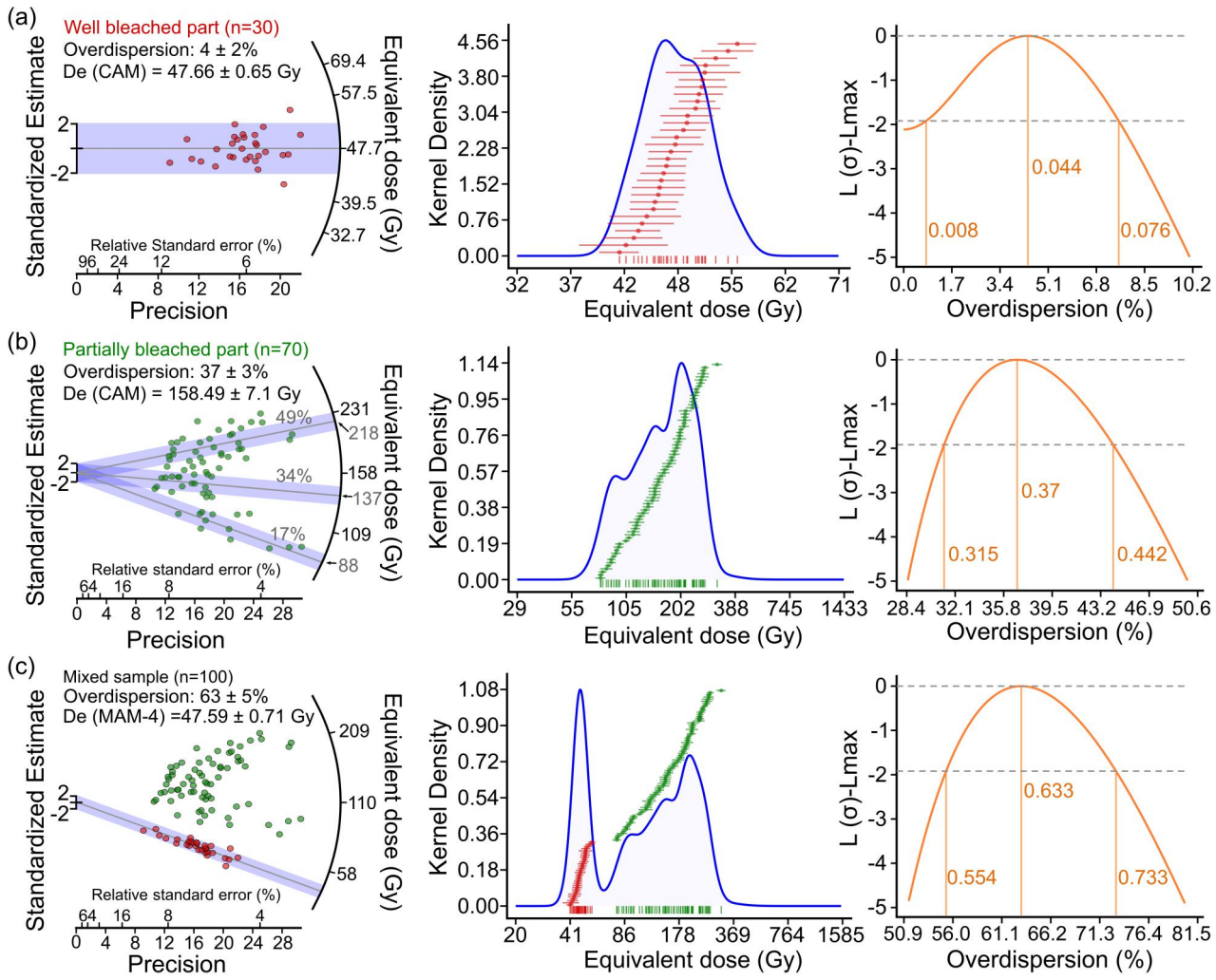

Figure 6. The unmixed (a and b) and mixed (c) simulant samples used in validation for Minimum Age Model (MAM). (a) shows equivalent dose distribution of a well solar reset component with 4 ± 2% overdispersion; (b) illustrates partially solar reset component which includes three sub-populations and with 37 ± 3% overdispersion. (c) Distribution of the mixed sample and the MAM-4 result.

As with the MAM, the MCMC slice sampling method (section 4.2.2) is used to estimate the upper truncation point, γ. The σ_b value is vital for the accuracy of MAX, and this value can be estimated from the associated parameters for well-bleached equivalent grains (Olley et al., 2006).

5. Environmental dose rate (D_r) and final age calculation

The environmental D_r of sediments that induces luminescence is from α, β and γ radiations from the radiative decay of the U and Th series, ^{40}K, ^{87}Rb and from cosmic-galactic components (Aitken 1985, chapter 4). The D_r is often calculated from the concentrations of radionuclides in the surrounding sediments within 30 cm radius of the sampling site based on the assumptions of an infinite matrix and secular equilibrium in the U and Th series (Aiken, 1998, p. 37–41; Guérin et al. 2012). The total environmental D_r for a particular grain size includes attenuation of external and internal dose contributions for grain-size, chemical etching of the alpha-affected outer 5 to 10 μm of grains and inferred sediment water content during the burial period, and cosmic dose components. The calculations for D_r in LDAC are similar to DRAC (Durcan et al., 2015), but with modifications discussed below.

5.1. Conversion and attenuation factors

LDAC offers three conversion factor options for dose contributions from α, β and γ components, as an infinite matrix dose, including 'Adamiec1998' (Adamiec & Aitken, 1998), 'Guérin2011' (Guérin et al., 2011) and 'Liritzis2013' (Liritzis et al., 2013) (worksheet 6 in Fig. 1). The given conversion factors assume secular equilibrium of U and Th decay series with no Radon loss (Aitken 1985, chapter 4). The uncertainties of the conversion factors derived from Liritzis et al. (2013) are applied proportional to the three data sets

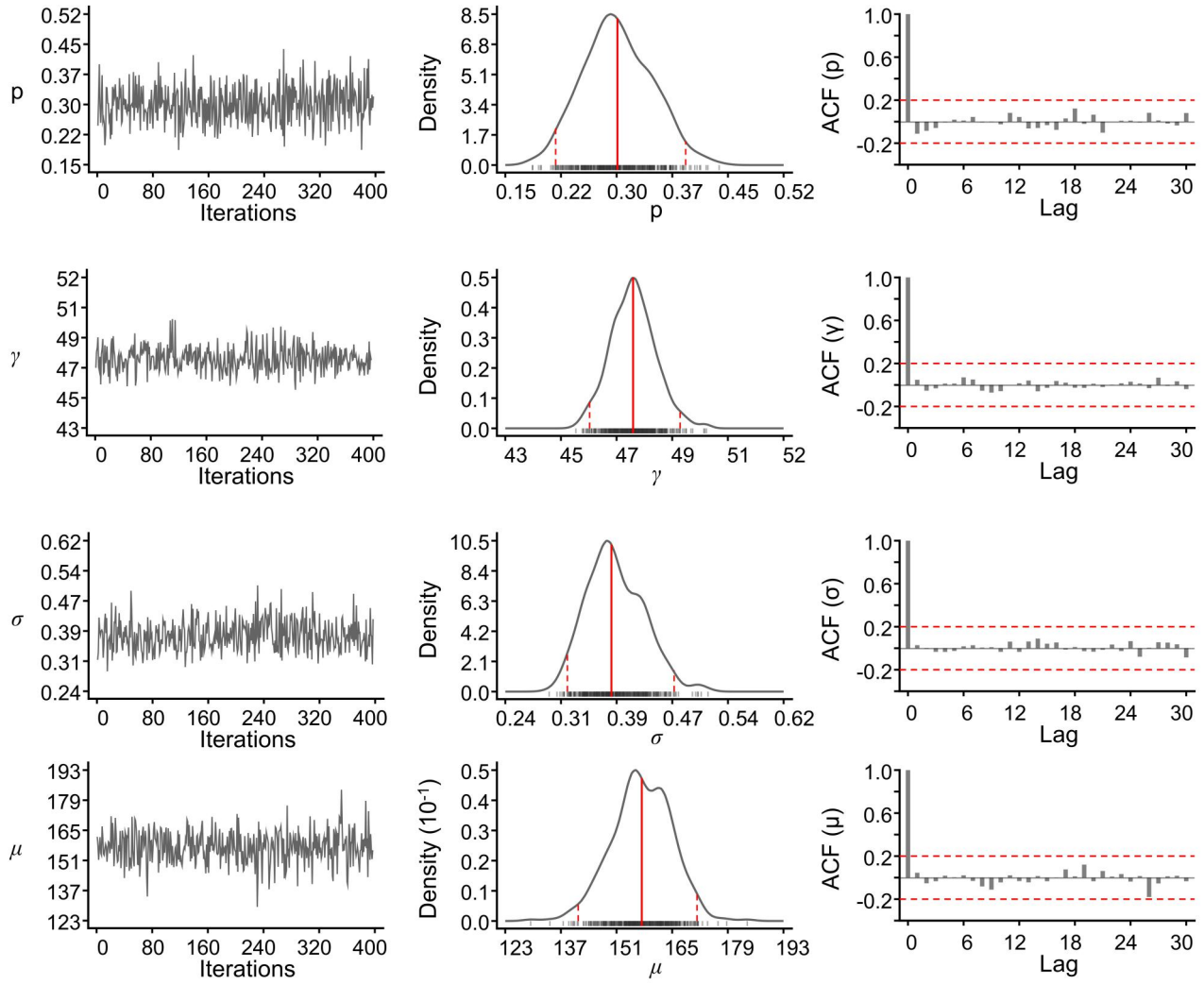

Figure 7. Estimation of the parameters p, γ, σ, and μ in minimum age model-4 for the simulant sample of Fig. 6c using the Markov chain Monte Carlo slice sampling method. The iteration times, burn-in, and thinning are 1800, 200 and 4, respectively.

following (Durcan et al., 2015). Users are required to input concentrations of U, Th, Rb in ppm and K or K_2O in % in the "Summary" page. The internal radionuclide concentration or dose rates and user-specified dose rates estimated through other methods, such as beta counting (Cunningham et al., 2018), can be input in the bottom panel of the "Summary" page and incorporated into subsequent attenuation as an option (Supplement A).

Several attenuation factors are considered in dose rate calculations including by grain size, from chemical etching (e.g., HF) of grain surface, by water content and a-value for alpha radiation (Aitken 1985, p. 252–263). Previously vetted attenuation factors are used in LDAC (e.g. Durcan et al. 2015) (worksheets 7-10 in Fig. 1). The default parameters for α and β attenuation by grain size and after chemical etching are from Brennan et al. (1991), Guérin et al. (2012), Bell (1980) and Brennan (2003), respectively. Alternative earlier parameters can be chosen on the "Summary" page (Supplement A) for β attenuation by grain size (Mejdahl, 1979; Brennan, 2003) to facilitate D_r comparison with previously published calculations. Grain size attenuation effects for α and β radiation is corrected with a resolution of 1 μm and a grain size range of 1 to 1000 μm (worksheet 7-8; Durcan et al. 2015). The factors and associated uncertainties are determined for the mean value and associated standard deviations corresponding to a grain size range (e.g., 150–250 μm). Similarly, the chemical etching attenuation factors are calculated with 1 μm resolution to a removal depth of 1 to 30 μm (worksheet 9-10; Durcan et al. 2015). A γ scaling factor is used to correct the contribution from inert air, for sediments collected at depths from < 30 cm of the ground surface (Aitken 1985, p. 289–296; Durcan et al. 2015; worksheet 11 in Fig. 1). These attenuated dry dose rates are adjusted for the water content with the attenuation factors for α, β and γ of 1.49, 1.25 and 1.14, respectively (Aitken 1985, p. 74–76; Grün 1994; Durcan et al. 2015).

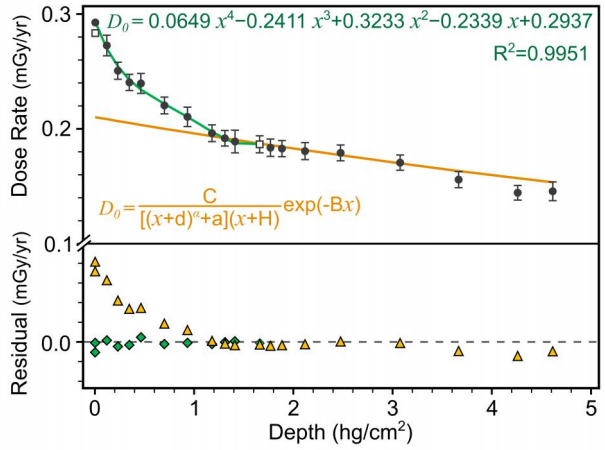

Figure 8. Standard cosmic dose rate (D_0) at different depths below surface. The black dots are the original measured data from bryozoan limestone in the southeast of South Australia (Prescott & Hutton, 1988). The white square data point at 1.67 hg/cm^2 is from Barbouti & Rastin (1983), and the white square at zero depth is from Kyker & Liboff (1978). The green and orange line show fitted curved defined by Eq. 24 and Eq. 25, respectively. The lower panel shows the D_0 residual between measured and fitted data. The constants of the equation are C = 6072, B = 5.50×10^{-4}, d = 11.6, α = 1.68, a = 75 and H = 212 (Prescott & Hutton, 1994).

5.2. Cosmic Dose Rate

The cosmic dose rate (D_c) is an integral part of the evaluation of the D_r, particularly for low dose sediments. The D_c calculation in LDAC follows the protocol outlined by Prescott & Hutton (1994). The standard cosmic dose rate (D_0) is calculated at sea level at a geomagnetic latitude of 55° for a given depth and overburden density using the following equations:

$$D_0 = 0.0649x^4 - 0.2411x^3 + 0.3233x^2 - 0.2339x + 0.2937, \quad x < 1.67 \text{ hg/cm}^2, \tag{24}$$

or

$$D_0 = \frac{6072}{[(x+11.6)^{1.68}+75](x+212)} e^{-0.00055x}, \quad x \geq 1.67 \text{ hg/cm}^2, \tag{25}$$

where x (hg/cm^2, equals to 100 g/cm^2) is the product of sampling depth below ground surface (m) and average overburden bulk density of the sediments (g/cm^3).

Eq. 25 from Prescott & Hutton (1994) is used to calculate D_0, but as pointed out by the authors, it is not valid for depths shallower than 1.67 hg/cm^2 (Aitken 1985, p. 297–298; Fig. 8). The principal components of the cosmic dose in the atmosphere are ionized electrons and muons, with a negligible contribution from heavier particles (Prescott & Hutton, 1988). The 'soft' component (electrons) of cosmic rays is attenuated with increasing depth into sediments, with penetrating limited at density depth of 1.5 ~ 1.67 hg/cm^2 (Barbouti & Rastin, 1983; Prescott & Hutton, 1988). The remaining 'hard' component (muons) is less readily attenuated, and it can penetrate to considerable depths, with decreasing intensity (Prescott & Hutton, 1988). The prototype of Eq. 25 is an empirical relationship between the vertical muon intensity and depth (Barbouti & Rastin, 1983), and only considers the 'hard' component of the cosmic rays. This equation (Eq. 25) excludes the 'soft' component (electron) of cosmic rays at depth shallower than 1.67 hg/cm^2 (Durcan et al., 2015; Burow, 2018). The residual between the 'hard' and 'soft' data sets for dose attenuation with depth is derived from measured cosmic dose from a bryozoan limestone in southeastern South Australia (orange triangles in Fig. 8). We translated the original measurement values from Figure 1 of Prescott and Hutton (1988) using MATLAB; the data points < 1.67 hg/cm^2 were fitted with a 4-degree polynomial function (Eq. 24; Fig. 8). LDAC adopts Eq. 24 to calculate the D_0 for depth between 0 and 1.67 hg/cm^2, because it includes both the 'soft' and 'hard' components in evaluating the cosmic dose rate, which is an accurate assessment.

The D_0 is then corrected by F, J and H values based on the geomagnetic latitude and altitude for the dated sediment (Prescott & Stephan, 1982; Durcan et al., 2015). The effect of known variations of the geomagnetic field is corrected for dose rate estimates for the late Pleistocene (Prescott & Hutton, 1994). Users can choose an estimated age range (0 – 5, 5 – 10, 10 – 15, 20 – 35, 35 – 50, 50 – 80 and > 80 ka) from the 'Age Estimate' tab (Fig. 9a) in the "Summary" worksheet. This value, together with altitude and the geomagnetic latitude converted from geographical coordinate, are applied to determine the geomagnetic field fluctuation factor (f_g) and altitude factor (f_h) (Prescott & Hutton 1994; Fig. 9). Consequently, the final equation for cosmic dose rate is:

$$D_c = D_0 \cdot (F + J \cdot e^{(h/1000)/H}) \cdot f_h \cdot (f_g - 1) \tag{26}$$

where F, J and H are the correction parameters of altitude and geomagnetic latitude (Prescott & Hutton, 1994; Durcan et al., 2015); h is the altitude of the sampling site (in m a.s.l.); f_g is the correction factors for cosmic ray flux change resulting from geomagnetic fields variations (Fig. 9a); and f_h is the factor for adjusting f_g for altitude (Fig. 9b). LDAC assigns an uncertainty of ± 10% for the calculated D_c (Prescott & Hutton, 1994). User-defined cosmic dose rate can also be input in the "Summary" page, if necessary.

The overburden density influences the accuracy of D_c calculation. LDAC allows users to input an estimated average bulk density different from the default value of 1.6 ± 0.1 g/cm^3, which is based on the investigation of soil dry bulk density, such as loess (1.1 – 1.8 g/cm^3) and aeolian sand (1.3 – 1.8 g/cm^3) with adjustments for field moisture content (Logsdon & Karlen, 2004; Wang et al., 2014).

5.3. Final Age calculation

The D_r is computed by the sum of all attenuated radionuclide components which include D_α^U, D_β^U, D_γ^U, D_α^{Th}, D_β^{Th},

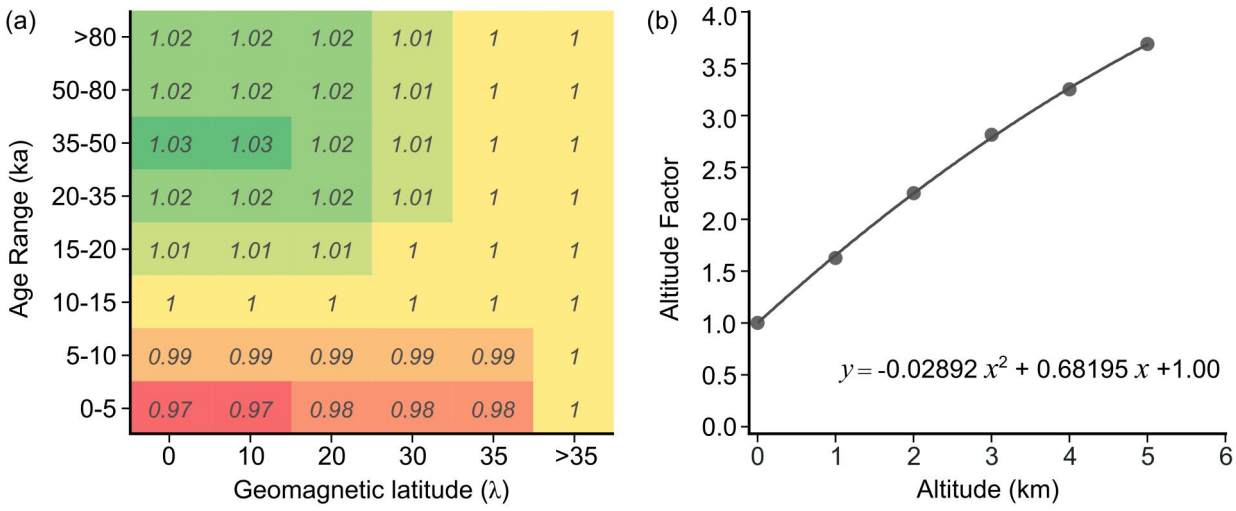

Figure 9. Correction factors for adjusting geomagnetic field variations for time (a) and altitude (b) (Prescott & Hutton, 1994).

D_γ^{Th}, D_β^K, D_γ^K, D_β^{Rb}, and the cosmic dose rate D_c. LDAC calculates the final age based on Eq. 1; the mean dose rate and age is calculated from mean values before rounding to two significant figures. The dose rate and associated uncertainty are reported in the "Summary" page at two significant figures (e.g., 2.75 mGy/yr). The final age is reported to the nearest 5-year increment if < 50 ka and rounded to the nearest 10-year increment for ages > 50 ka, reflecting inherent resolution.

5.4. Error propagation

LDAC provides two approaches to evaluate the uncertainties of the environmental dose rate and hence the final age. The first one is based on quadrature (Aitken 1985, p. 241–251; Taylor 1997, p. 45–92). However, all uncertainties propagated in quadrature will underestimate the total error because parts of dose rate from γ, β and α are correlated, which share the same source of errors from nuclide measurements (Grün 1994; Grün 2009; Taylor 1997, p. 45–92). To overcome this drawback, LDAC computes and attenuates the α, β and γ radiations from each nuclide independently in all steps and propagates the errors in quadrature separately in each step. Until the last step, all errors are combined based on:

$$\sigma_{D_r} = \sqrt{\begin{array}{l}\left(\sigma_{D_\alpha^U}+\sigma_{D_\beta^U}+\sigma_{D_\gamma^U}\right)^2+\left(\sigma_{D_\alpha^{\mathrm{Th}}}+\sigma_{D_\beta^{\mathrm{Th}}}+\sigma_{D_\gamma^{\mathrm{Th}}}\right)^2 \\ +\left(\sigma_{D_\beta^K}+\sigma_{D_\gamma^K}\right)^2+\left(\sigma_{D_\beta^{\mathrm{Rb}}}\right)^2+(\sigma_{D_c})^2\end{array}} \quad (27)$$

$$\sigma_{\mathrm{age}} = Age\sqrt{\left(\frac{\sigma_{D_e}}{D_e}\right)^2+\left(\frac{\sigma_{D_r}}{D_r}\right)^2}, \quad (28)$$

where $\sigma_{D_\beta^U}$ is the uncertainty of attenuated β dose rate (internal and external) emitted by U; it combines the random and systematic errors from nuclide measurement, conversion factors, attenuation factors and water content in quadrature. All other subscript of each σ has a corresponding meaning.

The second method for propagating the uncertainties in the final age estimate from all data sources is through Monte Carlo simulations. This approach is commonly used in numeric analysis to more faithfully propagate the uncertainties that are statistically robust (e.g., Anderson 1976; Duller 2007; Vermeesch 2007; Shao et al. 2014). This analysis assumes that each numeric value of input variables (e.g., U, Th, K, Rb, water contents), conversion and attenuation factors and their associated errors are represented by a Gaussian distribution of possible values. A large amount of repeated D_r and age calculations (e.g., 1000) are undertaken with stochastic values drawn from the independent Gaussian distributions (Shao et al., 2014). The 68.3% CI is evaluated by the 15.85 % and 84.15 % quantiles of outputs of the Monte Carlo simulations, and this asymmetric age interval is available in the final report (Supplement B). The 1σ uncertainties for the D_r and the final age are determined by the standard deviations of the Monte Carlo results (Cox, 2006). The default Monte Carlo iteration times in LDAC is 1000 which can be modified. This Monte Carlo simulation is a stochastic numeric analysis to propagate estimates of the total uncertainties, and thus these uncertainties will vary slightly with each calculation (Duller, 2007). The central values of D_r and OSL age are still calculated based on the input values rather than the mean of the Monte Carlo outputs.

5.5. Comparisons with other calculation packages

All algorithms for equivalent dose and dose rate calculations in LDAC are well developed by the community in the past thirty years. The key merit of the LDAC is assembling the most used functions for calculating the luminescence age to one package. To test the consistency between LDAC (v1.0) and other existing calculation tools, we compared both the D_e and D_r calculated by different published

Table 4. Comparison between equivalent doses (D_e) calculated by LDAC and **R** `'Luminescence'` package. BG4285 is the example data set of LDAC (v1.0) and the 'simulated sample' is the data set used in Section 4.2.3

Sample	Software	CAM		MAM	MAX
		D_e	Overdispersion		
BG4285	LDAC	366.05 ± 10.06	16.43 ± 2.03	325.68 ± 21.90	407.20 ± 27.92
	`'Luminescence'`	366.05 ± 10.06	16.43 ± 2.03	314.27 ± 17.48	NA
Simulated	LDAC	110.42 ± 7.02	63.30 ± 4.52	47.59 ± 0.71	237.22 ± 17.28
sample	`'Luminescence'`	110.42 ± 7.02	63.30 ± 4.52	47.54 ± 1.11	226.52 ± 9.81

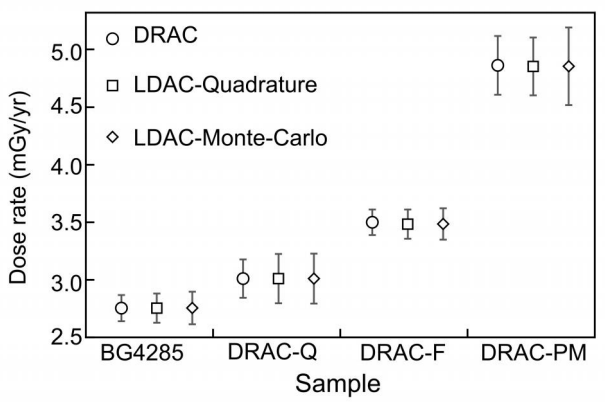

Figure 10. Comparison of dose rates (D_r) calculated by LDAC and DRAC. BG4285 is the example data set in LDAC (v1.0). DRAC-Q, DRAC-F and DRAC-PM are quartz, feldspar and poly-mineral example data sets provided by DRAC (Durcan et al., 2015), respectively. The raw data and used parameters are provided in Supplement D.

software. The comparisons show that our D_e and D_r are consistent with the results calculated by the **R** `'Luminescence'` package and the DRAC within the error range, respectively (Table 4; Fig. 10). However, the standard error of dose rate calculated by LDAC is systematically greater than that of DRAC (Fig. 10), which is caused by the different error propagation strategies stated in Section 5.4.

6. Discussion and Future direction

LDAC is a user-friendly, statistically robust, and self-contained luminescence age calculator which provides equivalent dose, environment dose rate, and final age calculations. This platform is accessible in a Windows environment equipped with Microsoft Excel 2010 or later. The framework of this software openly defines the calculation processes and input and output parameters. This Excel-based program, beyond a calculation tool, can be an effective manager of OSL data. Users can store the parameters of SAR sequences, individual aliquot or grain D_e values, dose rate information, pertinent diagnostic metrics on data quality and other analytical results as a separate LDAC file for each dated sediment. LDAC requires users to input or import their measured data just one time, which can reduce potential mistakes in exchanging data among multiple calculation programs.

This is the first generation of LDAC as an open-source and free access luminescence age calculation software. We plan to further develop and refine this software with advances in luminescence dating and community input. This calculation platform will also evolve for dating and research applications with improvements to the Microsoft Excel. The conversion and attenuation factors for dose rate calculation will be updated to reflect periodic refinements. Moreover, future additions of LDAC may include new statistical models (e.g., Guérin et al. 2017) for assessing disequilibrium of U and Th decay series and improved formulations for variations in cosmic and galactic radiation with fluctuations of Earth's magnetic field. Improving the calculation efficiency of Monte Carlo simulation is also a direction of future optimization.

Acknowledgments

This work was supported by the China Scholarship Council (awarded to P.L.), the National Natural Science Foundation of China (#41430532), the State Scientific Survey Project of China (#2017FY101001), USA National Science Foundation Award #GSS-1660230 (SLF), National Geographic Society Award #9990-16 (SLF), and the Geoluminescence Dating Research Laboratory at Baylor University, USA. Sincere thanks are extended to Liliana Marin for discussion and proofreading the manuscript and to Professor Geoff A.T. Duller for his very valuable comments and suggestions.

References

Adamiec, G. and Aitken, M. J. *Dose-rate conversion factors: update*. Ancient TL, 16: 37–50, 1998.

Ahr, S. W., Nordt, L. C., and Forman, S. L. *Soil genesis, optical dating, and geoarchaeological evaluation of two upland Alfisol pedons within the Tertiary Gulf Coastal Plain*. Geoderma, 192: 211–226, 2013.

Aitken, M. J. *Thermoluminescence dating*. Academic Press, Orlando, Florida, 1985.

Aitken, M. J. *Introduction to optical dating: the dating of Quaternary sediments by the use of photon-stimulated luminescence*. Oxford University Press, New York, 1998.

Anderson, G. *Error propagation by the Monte Carlo method in geochemical calculations.* Geochimica Cosmochimica Acta, 40: 1533–1538, 1976.

Arnold, L. J. and Roberts, R. G. *Stochastic modelling of multi-grain equivalent dose (De) distributions: Implications for OSL dating of sediment mixtures*. Quaternary Geochronology, 4: 204–230, 2009.

Arnold, L. J., Bailey, R. M., and Tucker, G. E. *Statistical treatment of fluvial dose distributions from southern Colorado arroyo deposits*. Quaternary Geochronology, 2: 162–167, 2007.

Arnold, L. J., Roberts, R. G., Galbraith, R. F., and DeLong, S. B. *A revised burial dose estimation procedure for optical dating of young and modern-age sediments*. Quaternary Geochronology, 4: 306–325, 2009.

Bailey, R. M. and Arnold, L. J. *Statistical modelling of single grain quartz De distributions and an assessment of procedures for estimating burial dose*. Quaternary Science Reviews, 25: 2475–2502, 2006.

Balco, G., Stone, J. O., Lifton, N. A., and Dunai, T. J. *A complete and easily accessible means of calculating surface exposure ages or erosion rates from ^{10}Be and ^{26}Al measurements*. Quaternary Geochronology, 3: 174–195, 2008.

Barbouti, A. and Rastin, B. *A study of the absolute intensity of muons at sea level and under various thicknesses of absorber*. Journal of Physics G: Nuclear Physics, 9: 1577, 1983.

Bell, W. *Alpha dose attenuation in quartz grains for thermoluminescence dating*. Ancient TL, 12: 4–8, 1980.

Bolker, B. and R Development Core Team. *bbmle: Tools for General Maximum Likelihood*. R package version, 1.0.20, 2017. URL https://CRAN.R-project.org/package=bbmle.

Botev, Z. I., Grotowski, J. F., and Kroese, D. P. *Kernel density estimation via diffusion*. Annals of Statistics, 38: 2916–2957, 2010.

Bøtter-Jensen, L., McKeever, S. W. S., and Wintle, A. G. *Optically stimulated luminescence dosimetry*. Elsevier, 2003.

Brennan, B. *Beta doses to spherical grains*. Radiation Measurements, 37: 299–303, 2003.

Brennan, B., Lyons, R., and Phillips, S. *Attenuation of alpha particle track dose for spherical grains*. International Journal of Radiation Applications and Instrumentation. Part D. Nuclear Tracks and Radiation Measurements, 18: 249–253, 1991.

Brooks, S., Gelman, A., Jones, G., and Meng, X.-L. *Handbook of Markov chain Monte Carlo*. CRC Press, 2011.

Burow, C. *calc_ CosmicDoseRate(): Calculate the cosmic dose rate. Function version 0.5.2*. In Kreutzer, S., Burow, C., Dietze, M., Fuchs, M., Schmidt, C., Fischer, M., and Friedrich, J. (eds.), *Luminescence: Comprehensive Luminescence Dating Data Analysis. R package version 0.8.6*. 2018. URL https://CRAN.R-project.org/package=Luminescence.

Burow, C., Kreutzer, S., Dietze, M., Fuchs, M. C., Fischer, M., Schmidt, C., and Brückner, H. *RLumShiny-A graphical user interface for the R Package 'Luminescence'*. Ancient TL, 34: 22–32, 2016.

Cowles, M. K. and Carlin, B. P. *Markov chain Monte Carlo convergence diagnostics: a comparative review.* Journal of the American Statistical Association, pp. 883–904, 1996.

Cox, D. *Principles of statistical inference*. Cambridge University Press, New York, 2006.

Cunningham, A. C. and Wallinga, J. *Realizing the potential of fluvial archives using robust OSL chronologies*. Quaternary Geochronology, 12: 98–106, 2012.

Cunningham, A. C., Murray, A. S., Armitage, S. J., and Autzen, M. *High-precision natural dose rate estimates through beta counting*. Radiation Measurements, 120: 209–214, 2018.

Duller, G. A. T. *Distinguishing quartz and feldspar in single grain luminescence measurements*. Radiation Measurements, 37: 161–165, 2003.

Duller, G. A. T. *Assessing the error on equivalent dose estimates derived from single aliquot regenerative dose measurements*. Ancient TL, 10: 15–24, 2007.

Duller, G. A. T. *The Analyst software package for luminescence data: overview and recent improvements*. Ancient TL, 33: 35–42, 2015.

Duller, G. A. T. *Enhancing Analyst by integrating the R package 'Luminescence'*. Ancient TL, 36: 1–6, 2018.

Durcan, J. A. and Duller, G. A. T. *The fast ratio: A rapid measure for testing the dominance of the fast component in the initial OSL signal from quartz*. Radiation Measurements, 46: 1065–1072, 2011.

Durcan, J. A., King, G. E., and Duller, G. A. T. *DRAC: Dose Rate and Age Calculator for trapped charge dating*. Quaternary Geochronology, 28: 54–61, 2015.

Forman, S. L. *Episodic eolian sand deposition in the past 4000 years in Cape Cod National Seashore, Massachusetts, USA in response to possible hurricane/storm and anthropogenic disturbances*. Frontiers in Earth Sciences, 3: 3, 2015.

Forman, S. L., Tripaldi, A., and Ciccioli, P. L. *Eolian sand sheet deposition in the San Luis paleodune field, western Argentina as an indicator of a semi-arid environment through the Holocene.* Palaeogeography, Palaeoclimatology, Palaeoecology, 411: 122–135, 2014.

Galbraith, R., Roberts, R., and Yoshida, H. *Error variation in OSL palaeodose estimates from single aliquots of quartz: a factorial experiment*. Radiation Measurements, 39: 289–307, 2005.

Galbraith, R. F. *Graphical display of estimates having differing standard errors*. Technometrics, 30: 271–281, 1988.

Galbraith, R. F. *The radial plot: graphical assessment of spread in ages*. International Journal of Radiation Applications and Instrumentation. Part D. Nuclear Tracks and Radiation Measurements, 17: 207–214, 1990.

Galbraith, R. F. *A simple homogeneity test for estimates of dose obtained using OSL*. Ancient TL, 21: 75–77, 2003.

Galbraith, R. F. *Statistics for fission track analysis*. Chapman and Hall/CRC, 2005.

Galbraith, R. F. *On plotting OSL equivalent doses*. Ancient TL, 28: 1–10, 2010.

Galbraith, R. F. and Green, P. *Estimating the component ages in a finite mixture*. International Journal of Radiation Applications and Instrumentation. Part D. Nuclear Tracks and Radiation Measurements, 17: 197–206, 1990.

Galbraith, R. F. and Roberts, R. G. *Statistical aspects of equivalent dose and error calculation and display in OSL dating: an overview and some recommendations*. Quaternary Geochronology, 11: 1–27, 2012.

Galbraith, R. F., Roberts, R. G., Laslett, G. M., Yoshida, H., and Olley, J. M. *Optical dating of single and multiple grains of quartz from Jinmium rock shelter, northern Australia: Part I, experimental design and statistical models*. Archaeometry, 41: 339–364, 1999.

Gelfand, A. E. and Smith, A. F. *Sampling-based approaches to calculating marginal densities*. Journal of the American Statistical Association, 85: 398–409, 1990.

Gilks, W. R., Best, N., and Tan, K. *Adaptive rejection Metropolis sampling within Gibbs sampling*. Journal of the Royal Statistical Society. Series C (Applied Statistics), 44: 455–472, 1995.

Gilks, W. R., Richardson, S., and Spiegelhalter, D. *Markov chain Monte Carlo in practice*. Springer-Science+Business Media, Dordrecht, 1996.

Grün, R. *A cautionary note: use of 'water content' and 'depth for cosmic ray dose rate' in AGE and DATA programs*. Ancient TL, 12: 50–51, 1994.

Grün, R. *The "AGE" program for the calculation of luminescence age estimates*. Ancient TL, 27: 45–46, 2009.

Guérin, G., Mercier, N., and Adamiec, G. *Dose-rate conversion factors: update*. Ancient TL, 29: 5–8, 2011.

Guérin, G., Mercier, N., Nathan, R., Adamiec, G., and Lefrais, Y. *On the use of the infinite matrix assumption and associated concepts: A critical review*. Radiation Measurements, 47: 778–785, 2012.

Guérin, G., Jain, M., Thomsen, K. J., Murray, A. S., and Mercier, N. *Modelling dose rate to single grains of quartz in well-sorted sand samples: The dispersion arising from the presence of potassium feldspars and implications for single grain OSL dating*. Quaternary Geochronology, 27: 52–65, 2015.

Guérin, G., Christophe, C., Philippe, A., Murray, A. S., Thomsen, K. J., Tribolo, C., Urbanova, P., Jain, M., Guibert, P., Mercier, N., Kreutzer, S., and Lahaye, C. *Absorbed dose, equivalent dose, measured dose rates, and implications for OSL age estimates: Introducing the Average Dose Model*. Quaternary Geochronology, 41: 163–173, 2017.

Hesse, P. P., Williams, R., Ralph, T. J., Fryirs, K. A., Larkin, Z. T., Westaway, K. E., and Farebrother, W. *Palaeohydrology of lowland rivers in the Murray-Darling Basin, Australia*. Quaternary Science Reviews, 200: 85–105, 2018.

Huntley, D. J., Godfrey-Smith, D. I., and Thewalt, M. L. W. *Optical dating of sediments*. Nature, 313: 105–107, 1985.

Jacobs, Z. and Roberts, R. G. *Advances in optically stimulated luminescence dating of individual grains of quartz from archeological deposits*. Evolutionary Anthropology, 16: 210–223, 2007.

Jones, R. S., Small, D., Cahill, N., Bentley, M. J., and Whitehouse, P. L. *iceTEA: Tools for plotting and analysing cosmogenic-nuclide surface-exposure data from former ice margins*. Quaternary Geochronology, 51: 72–86, 2019.

Kreutzer, S., Schmidt, C., Fuchs, M. C., Dietze, M., Fischer, M., and Fuchs, M. *Introducing an R package for luminescence dating analysis*. Ancient TL, 30: 1–8, 2012.

Kreutzer, S., Burow, C., Dietze, M., Fuchs, M. C., Schmidt, C., Fischer, M., and Friedrich, J. *Luminescence: Comprehensive Luminescence Dating Data Analysis. R package version 0.8.6*, 2018. URL https://CRAN.R-project.org/package=Luminescence.

Kyker, G. C. and Liboff, A. R. *Absolute cosmic ray ionization measurements in a 900-liter chamber*. Journal of Geophysical Research: Space Physics, 83: 5539–5549, 1978.

Lancaster, N., Wolfe, S., Thomas, D., Bristow, C., Bubenzer, O., Burrough, S., Duller, G. A. T., Halfen, A., Hesse, P., Roskin, J., Singhvi, A., Tsoar, H., Tripaldi, A., Yang, X., and Zárate, M. *The INQUA Dunes Atlas chronologic database*. Quaternary International, 410: 3–10, 2016.

Lang, A., Hatté, C., Rousseau, D. D., Antoine, P., Fontugne, M., Zöller, L., and Hambach, U. *High-resolution chronologies for loess: comparing AMS 14C and optical dating results*. Quaternary Science Reviews, 22: 953–959, 2003.

Liritzis, I., Stamoulis, K., Papachristodoulou, C., and Ioannides, K. *A re-evaluation of radiation dose-rate conversion factors*. Mediterranean Archaeology and Archaeometry, 13: 1–15, 2013.

Logsdon, S. D. and Karlen, D. L. *Bulk density as a soil quality indicator during conversion to no-tillage*. Soil Tillage Research, 78: 143–149, 2004.

Ludwig, K. R. *ISOPLOT for MS-DOS, a Plotting and Regression Program for Radiogenic Isotope Data for IBM-PC Compatible Computers, Version 1.00. USGS Open-File Report OF-88-0557*, 1988.

Mejdahl, V. *Thermoluminescence dating: beta-dose attenuation in quartz grains*. Archaeometry, 21: 61–72, 1979.

Murray, A. S. and Wintle, A. G. *Luminescence dating of quartz using an improved single-aliquot regenerative-dose protocol*. Radiation Measurements, 32: 57–73, 2000.

Murray, A. S. and Wintle, A. G. *The single aliquot regenerative dose protocol: potential for improvements in reliability*. Radiation Measurements, 37: 377–381, 2003.

Neal, R. M. *Slice sampling*. Annals of Statistics, 31: 705–767, 2003.

Olley, J. M., Roberts, R. G., Yoshida, H., and Bowler, J. M. *Single-grain optical dating of grave-infill associated with human burials at Lake Mungo, Australia*. Quaternary Science Reviews, 25: 2469–2474, 2006.

Peng, J., Dong, Z., Han, F., Long, H., and Liu, X. *R package numOSL: numeric routines for optically stimulated luminescence dating*. Ancient TL, 31: 41–48, 2013.

Philippe, A., Guérin, G., and Kreutzer, S. *BayLum-An R package for Bayesian analysis of OSL ages: An introduction*. Quaternary Geochronology, 49: 16–24, 2019.

Plummer, M., Best, N., Cowles, K., and Vines, K. *CODA: convergence diagnosis and output analysis for MCMC*. R news, 6: 7–11, 2006.

Prescott, J. and Stephan, L. *The contribution of cosmic radiation to the environmental dose for thermoluminescence dating: latitude, altitude and depth dependences*. PACT, 6: 17–25, 1982.

Prescott, J. R. and Hutton, J. T. *Cosmic ray and gamma ray dosimetry for TL and ESR*. International Journal of Radiation Applications and Instrumentation. Part D. Nuclear Tracks and Radiation Measurements, 14: 223–227, 1988.

Prescott, J. R. and Hutton, J. T. *Cosmic ray contributions to dose rates for luminescence and ESR dating: Large depths and long-term time variations*. Radiation Measurements, 23: 497–500, 1994.

Preusser, F., Chithambo, M. L., Götte, T., Martini, M., Ramseyer, K., Sendezera, E. J., Susino, G. J., and Wintle, A. G. *Quartz as a natural luminescence dosimeter*. Earth-Science Reviews, 97: 184–214, 2009.

Ramsey, C. B. *Radiocarbon calibration and analysis of stratigraphy: the OxCal program*. Radiocarbon, 37: 425–430, 1995.

Ramsey, C. B. *Methods for Summarizing Radiocarbon Datasets*. Radiocarbon, 59: 1809–1833, 2017.

Rodnight, H. *How many equivalent dose values are needed to obtain a reproducible distribution*. Ancient TL, 26: 3–9, 2008.

Shao, Q., Bahain, J.-J., Dolo, J.-M., and Falguères, C. *Monte Carlo approach to calculate US-ESR age and age uncertainty for tooth enamel*. Quaternary Geochronology, 22: 99–106, 2014.

Silverman, B. W. *Density estimation for statistics and data analysis*. Routledge, 1998.

Sircombe, K. N. *AgeDisplay: an EXCEL workbook to evaluate and display univariate geochronological data using binned frequency histograms and probability density distributions*. Computers & Geosciences, 30: 21–31, 2004.

Stuiver, M., Reimer, P. J., and Reimer, R. W. *CALIB 7.1 [WWW program] at*, 2019. URL http://calib.org. accessed 2019-6-16.

Tabachnick, B. G. and Fidell, L. S. *Using Multivariate Statistics (3rd ed.)*. Harper and Row, New York, NY, USA, 1996.

Tamura, T., Cunningham, A. C., and Oliver, T. S. N. *Two-dimensional chronostratigraphic modelling of OSL ages from recent beach-ridge deposits, SE Australia*. Quaternary Geochronology, 49: 39–44, 2019.

Taylor, J. *An Introduction to error analysis: the study of uncertainties in physical measurements*. University Science Books, Sausalito, California, 1997.

Vermeesch, P. *CosmoCalc: An Excel add-in for cosmogenic nuclide calculations*. Geochemistry, Geophysics, Geosystems, 8: Q08003, 2007. doi: 10.1029/2006GC001530.

Vermeesch, P. *On the visualisation of detrital age distributions*. Chemical Geology, 312: 190–194, 2012.

Vermeesch, P. *Dissimilarity measures in detrital geochronology*. Earth-Science Reviews, 178: 310–321, 2018.

Wang, Y., Shao, M., Liu, Z., and Zhang, C. *Prediction of bulk density of soils in the Loess Plateau region of China*. Surveys in Geophysics, 35: 395–413, 2014.

Wintle, A. G. *Luminescence dating: where it has been and where it is going*. Boreas, 37: 471–482, 2008.

Wintle, A. G. and Adamiec, G. *Optically stimulated luminescence signals from quartz: A review*. Radiation Measurements, 98: 10–33, 2017.

Wintle, A. G. and Murray, A. S. *A review of quartz optically stimulated luminescence characteristics and their relevance in single-aliquot regeneration dating protocols*. Radiation Measurements, 41: 369–391, 2006.

Yang, X., Scuderi, L. A., Wang, X., Scuderi, L. J., Zhang, D., Li, H., Forman, S., Xu, Q., Wang, R., Huang, W., and Yang, S. *Groundwater sapping as the cause of irreversible desertification of Hunshandake Sandy Lands, Inner Mongolia, northern China.* Proceedings of the National Academy of Sciences of the United States of America, 112: 702–706, 2015.

Yang, X., Liang, P., Zhang, D., Li, H., Rioual, P., Wang, X., Xu, B., Ma, Z., Liu, Q., Ren, X., Hu, F., He, Y., Rao, G., and Chen, N. *Holocene aeolian stratigraphic sequences in the eastern portion of the desert belt (sand seas and sandy lands) in northern China and their palaeoenvironmental implications*. Science China Earth Sciences, 62: 1302–1315, 2019.

Reviewer

Geoff Duller

Reviewer comment:

This excellent paper is a welcome addition to the suite of software available for luminescence dating, and draws together a range of calculations that would otherwise be scattered across different programmes. The authors' parameterisation of the soft component of the cosmic dose rate (Eq. 24) is similar to that originally developed by Robert Clark in 1997 for his unpublished software "Cosmic". In that software he parameterised the data from Prescott & Hutton (1988) with the following function which was adopted for DRAC by Durcan et al. (2015).

$$D_c = 3.21 \times 10^{-2} x^4 - 1.35 \times 10^{-1} x^3 + 2.21 \times 10^{-1} x^2 - 2.07 \times 10^{-1} x + 0.295$$